ORIGINAL RESEARCH

Hypercholesterolemia Induces Oxidant Stress That Accelerates the Ageing of Hematopoietic Stem Cells

Guodong Tie, PhD; Katharine E. Messina, BA; Jinglian Yan, PhD; Julia A. Messina, MD; Louis M. Messina, MD

***Background*—**Clinical studies suggest that hypercholesterolemia may cause ageing in hematopoietic stem cells (HSCs) because ageing-associated alterations were found in peripheral blood cells and their bone marrow residing precursors in patients with advanced atherosclerosis. We hypothesized that hypercholesterolemia induces oxidant stress in hematopoietic stems cells that accelerates their ageing.

***Methods and Results*—**Here we show that HSCs from ApoE$^{-/-}$ mice, as well as HSCs from C57Bl/6 mice fed a high cholesterol diet (HCD) accumulated oxLDL and had greater ROS levels. In accordance, the expression pattern of the genes involved in ROS metabolism changed significantly in HSCs from ApoE$^{-/-}$ mice. Hypercholesterolemia caused a significant reduction in phenotypically defined long-term HSC compartment, telomere length, and repopulation capacity of KTLS cells, indicating accelerated ageing in these cells. Gene array analysis suggested abnormal cell cycle status, and the key cell cycle regulators including p19^{ARF}, p27^{Kip1} and p21^{Waf1} were upregulated in KTLS cells from hypercholesterolemic mice. These effects were p38-dependent and reversed in vivo by treatment of hypercholesterolemic mice with antioxidant *N*-acetylcysteine. The oxidant stress also caused aberrant expression of Notch1 that caused loss of quiescence and proliferation leading to the expansion of KTLS compartment in hypercholesterolemic mice.

***Conclusion*—**Taken together, we provide evidence that hypercholesterolemia can cause oxidant stress that accelerates the ageing and impairs the reconstitution capacity of HSCs. **(*J Am Heart Assoc*. 2014;3:e000241 doi: 10.1161/JAHA.113.000241)**

Key Words: ageing • hematopoietic stem cell • hypercholesterolemia • oxidant stress

Hypercholesterolemia is recognized as a major risk factor for cardiovascular disease and increases all-cause mortality in different epidemiological studies.[1–3] Little is known about the detrimental effects of hypercholesterolemia on hematopoietic stem cells (HSCs). Clinical investigations and basic research have implied that hypercholesterolemia acclerates ageing of HSCs. The first evidence was the finding of shorter telomeres in peripheral blood leukocytes of human patients with advanced atherosclerosis.[4] Spyridopoulos et al showed that the telomere length of peripheral white blood cells in patients with atherosclerotic disease correlates with the telomere lengths of their bone marrow-residing hematopoietic precursors.[5] Shortening of telomeres is recognized as one of the major ageing-associated alterations responsible for the loss of regenerative potential in tissues,[6] and is also linked to the initiation and/or progression of cardiovascular disease.[7] The other evidence indicated that hypercholesterolemia skewed myeloid lineage differentiation in human patients, which has been closely related to ageing of HSCs.[8,9] Hypercholesterolemic mice deficient in ABCA1 and ABCG1 displayed a dramatic expansion of HSC compartment and in the bone marrow.[10] ApoE-deficient mice fed a western diet developed the same prominent expansion of the HSC compartment in the bone marrow.[11] These mouse models also displayed myeloproliferative disorder. These abnormal alterations in HSCs suggest that hypercholesterolemia may cause ageing of HSCs, but the mechanism by which hypercholesterolemia causes these effects remains unknown.

In the present study, we found that hypercholesterolemia induces oxidant stress in HSCs that alters their gene expression and cell cycle regulation. Together these effects lead to ageing of HSCs manifested by telomere erosion, loss of quiescence, reduction in long-term HSC compartment, and impaired reconstitution capacity of HSCs.

From the Division of Vascular and Endovascular Surgery, University of Massachusetts Medical School, Worcester, MA (G.T., K.E.M., J.Y., L.M.M.); Division of Infectious Diseases, Duke University School of Medicine, Durham, NC (J.A.M.).

Correspondence to: Louis M. Messina, MD, Department of Surgery, 55 Lake Avenue North, Worcester, MA 01655. E-mail: Louis.Messina@umassmemorial.org

Received October 28, 2013; accepted December 16, 2013.

Materials and Methods

Mice

All mice were purchased from Jackson Laboratories and were maintained in the mouse barrier facility. Care of mice was in accordance with NIH guidelines and the Institutional Animal Care and Use Committee of the University of Massachusetts Medical School approved all protocols. Mice were kept on a 12-hour day/night schedule and were allowed free access to chow and water. ApoE$^{-/-}$ and WT mice were fed standard mouse chow (5.4 g fat/100 g diet, 0% cholesterol). HCD mice were fed a diet with 20 g fat/100 g diet, 11.25 g cholesterol/100 g diet (Research Diets). *N*-acetylcysteine (NAC) was given by intraperitoneal injection (150 mg/kg body weight every other day for 8 weeks). GSH (500 mg/kg body weight) and SB203580 (15 mg/kg body weight) were administered by intraperitoneal injection 3 times a week for 4 weeks.

Flow Cytometry

Cells were stained with monoclonal antibodies conjugated to various fluoroprobes. These antibodies included: Notch1, cKit (2B8), Sca-1 (E13-161.7), CD41, CD48, CD90.1, CD45.1, CD45.2, and lineage antibody cocktail. All antibodies were purchased from BD Bioscience. FACS analysis was carried out on a FACS Diva or MoFlow. The side population and Pyronin Y staining was performed as described.

Preparation of Lentiviral Particles

The pLenti expression plasmids were purchased from Open Biosystems. Second generation packing system was purchased from Applied Biosystems. Lentiviral particles were produced by transient transfection with 293T cells as indicated by manufacture protocol.

In Vitro Culture of HSCs

KTLS cells were cultured in Minimum Essential Media alpha modification (αMEM Sigma) containing 12.5% FCS (JRH Bioscience), 12.5% horse serum (Gibco BRL) and 1 nmol/L dexamethasone. For some experiments, we added 10 μmol/L SB203580 or 5 μmol/L γ secretase inhibitor XII (Calbiochem) into culture medium.

Immunocytochemistry

We used a standard cytocentrifuge protocol to detect nitrotyrosine and oxLDL in HSCs. The antibody against oxidized phospholipids with a phosphopcholine headgroup was a gift from J. Witztum (University of California San Diego). The antibody against nitrotyrosine was purchased from Cell Signaling Technology. We used rabbit-specific IgG conjugated with FITC (Invitrogen) as a secondary antibody. For nuclear staining, we treated specimens with DAPI (Molecular Probes). Fluorescent images were obtained using a confocal laser-scanning microscope (Carl Zeiss LSM 510 system; Carl Zeiss).

Competitive Bone Marrow Reconstitution Assay

We sorted KTLS cells from wild-type or ApoE$^{-/-}$ mice (CD45.2). We transplanted cells into lethally irradiated CD45.1 congenic mice in competition with HSCs from CD45.1 mice. We monitored reconstitution of donor (CD45.2) myeloid and lymphoid cells by staining blood cells with antibodies against CD45.2, CD45.1, CD3, B220, Mac-1, and Gr-1.

Sample Generation and DNA Microarray Hybridization and Analysis

KTLS cells were isolated as described. For the purpose of this assay only, KTLS cells pooled from 4 to 5 mice were used to generate a single KTLS sample. Total RNA was isolated using RNeasy Micro kit according to manufacturer's instructions (Qiagen). Total RNA was amplified in 2 rounds using the Amino Allyl MessageAmpII kit (Ambion). Five micrograms of amplified RNA, quantified using a NanoDrop ND-100 spectrophotometer (NanoDrop Technologies), was dried and then coupled to a fluorescent dye (Cy3 or Cy5). Equal amounts of Cy3 or Cy5 labeled aRNA (825 ng) obtained from 2 different samples (ApoE$^{-/-}$ or WT) were hybridized to Agilent Mouse Whole Genome Microarrays 4×44K for 17 hours at 65°C. The hybridized microarrays were washed and scanned using an Agilent G250B scanner. Four microarrays were carried out on RNA samples from discrete groups of ApoE$^{-/-}$ and WT mice, including one dye swap array. Data were extracted from the scanned image for preprocessing and normalization with Feature Extraction Software (v 9.5.3.1; Agilent Technologies, Inc). Data used for further analysis came from green and red Processed Signal values, generated after background subtraction and LOWESS normalization. Fold change was calculated as the ratio of red to green signal intensity. A list of candidate genes was identified, which demonstrated an average >2-fold increase or decrease in expression. The list was created from a filtered set of the data that included genes that were >1.5-fold changed in the same direction, in 4/4 microarrays. Data were further processed using GeneSpring GX software (Agilent Technologies, Inc) and Ingenuity Pathway Analysis (Ingenuity® Systems, www.ingenuity.com).

Analysis of Intracellular ROS

We loaded samples of cultures with DCF-DA (Sigma) and incubated them on a shaker at 37°C for 30 min. The peak

excitation wavelength for oxidized DCF was 488 nm, and emission was 525 nm. The concentration of H_2O_2 was measured by Amplex Red Hydrogen Peroxide/Peroxidase Assay Kit (Molecular Probes).

RT–PCR and qRT-PCR Array

RNA was isolated from cells using RNAqueous-Micro kit (Ambion Life Technologies). Transcription to cDNA was performed using SuperScript III (Invitrogen). The primers were purchased from Operon. The expression of ROS genes was detected by Mouse Oxidant Stress and Antioxidant Defense PCR Array (SABiosciences). All PCRs were carried out in triplicate using an Eppendorf Mastercycler (Eppendorf). Primer sequences are shown in Table 1.

Telomere Length Measurement

Telomere length was measured by telomere PNA kit/FITC (DAKO). In brief, the sample DNA was denatured for 10 minutes at 82°C in a microcentrifuge tube either in the presence of hybridization solution without probe or in hybridization solution containing fluorescein-conjugated PNA telomere probe. Then hybridization took place in the dark at room temperature (RT) overnight. The hybridization was followed by two 10-minute post-hybridization washes with a Wash Solution at 40°C. The sample was then resuspended in an appropriate buffer for further flow cytometric analysis. DNA Staining Solution included in the kit was used for identification of G0/1 cells. After flow cytometric analysis, the data obtained were used for determination of a relative telomere length (RTL). The RTL value was calculated as the ratio between the telomere signal of each sample and the control cell (1301 cell line) with correction for the DNA index of G0/1 cells.

Table 1. Primers Used in qRT-PCR Experiments

Gene	Primers
18s	Forward: CGGCTACCACATCCAAGGAA
	Reverse: GCTGGAATTACCGCGGCT
P19	Forward: CGGTATCCACTATGCTTCTGGAA
	Reverse: CCGCTGCGCCACTCAA
P21	Forward: TTCCGCACAGGAGCAAAGT
	Reverse: CGGCGCAACTGCTCACT
P27	Forward: GGCCCGGTCAATCATGAA
	Reverse: TTGCGCTGACTCG CTTCTTC
Notch1	Forward: ATGCTGCTGTTGTGCTCCT
	Reverse: CAGTCTCATAGCTGCCCTCAC
SR-A	Forward: TGGTCCACCTGGTGCTCC
	Reverse: ACCTCCAGGGAAGCCAAT TT
CD36	Forward: CAGTTGGAGACCTGCTTATCC
	Reverse: GCGTCCTGGGTTACATTTTC
LOX-1	Forward: GGCCAACCATGGCTTGGGAGAATGG
	Reverse: CAGCGAACACAGCTCCGTCTTGAAGG
CD68	Forward: GTCCTGGCTGTGTTTGGAGG
	Reverse: CTGTGCCATTAATCATGTCGCA
SR-B1	Forward: ACAACGACACCGTGTCCTTC
	Reverse: GAAGCCTTCGTTGGGTGGGTAGA
SR-B2	Forward: TTACCAAGCCGACGAGAAGT
	Reverse: ACCAAGCCAAAGAACACACC

LOX-1 indicates lectin-like oxidized low-density lipoprotein receptor 1; PCR, polymerase chain reaction; SR, scavenger receptors.

Statistical Analysis

All data were shown as means±SD. Statistical analyses were carried out with either GraphPad Prism (GraphPad Software) or SPSS v19 (IBM) software. Statistical significance was evaluated by using a 1- or 2-way analysis of variance (ANOVA) or an unpaired *t* test. Significance was established for *P* values <0.05. Adjustment for multiplicity of comparisons was not utilized.

Results

Hypercholesterolemia Causes Loss of Quiescence, Induces Proliferation and Accelerates Ageing in HSCs

We first investigated the effect of hypercholesterolemia on the key functions of hematopoietic stem cells. HSCs ($cKit^+sca\text{-}1^+CD90.1^{lo/-}Lin^-$, KTLS) were purified by multiparameter flow cytometer from B6.129P2-*Apoe*^{tmiUnc}/J mice ($ApoE^{-/-}$ mice), C57Bl/6 (WT mice), and C57Bl/6 mice fed a high cholesterol diet (1.25% cholesterol) for 8 weeks beginning at 1 month of age (HCD mice). The fasting total serum cholesterol concentration, measured in 3-month-old mice, was: WT 50±11 mg/dL; $ApoE^{-/-}$ 204±24 mg/dL*, HCD 243±21 mg/dL* (M±SD, n=7, *P<0.05 versus WT mice). The frequency of KTLS cells in $ApoE^{-/-}$ mice was 0.101±0.009% of total bone marrow cells, 2-fold higher than in WT mice (Figure 1A). Long-term HSCs (LT-HSCs), phenotypically defined as $CD34^-Flk_2^-$KTLS, were 20.53±2.63% of total KTLS in WT mice, but decreased to 7.93±0.821% in $ApoE^{-/-}$ mice (Figure 1B). Telomere length was significantly shorter in KTLS cells isolated from $ApoE^{-/-}$ mice than KTLS cells from WT mice (Figure 1C). As well, the proportion of the highly purified side population of total KTLS cells in $ApoE^{-/-}$ mice was significantly lower than that in WT mice (Figure 1D).

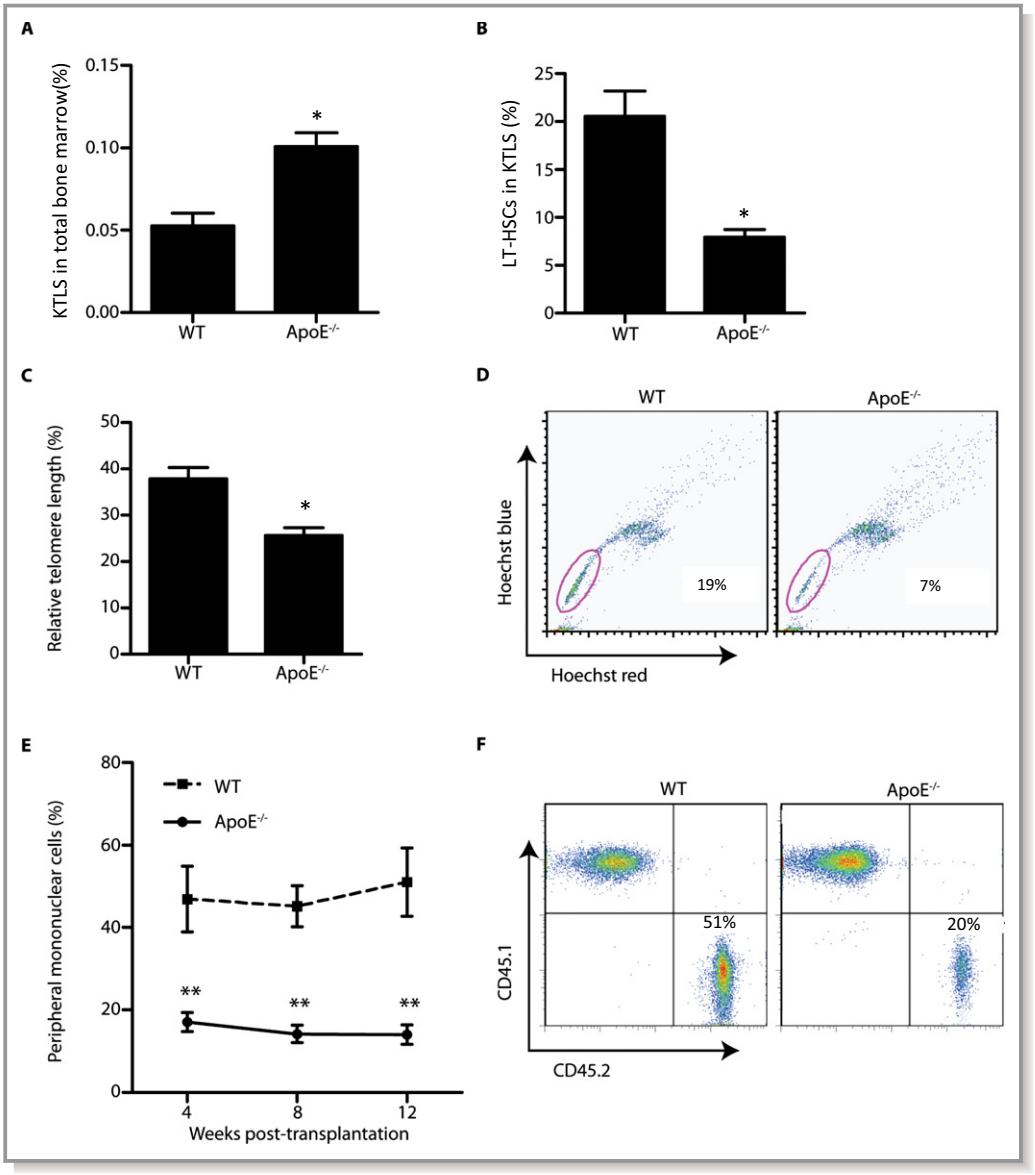

Figure 1. Hypercholesterolemia accelerates the ageing of HSC. A, The number of KTLS cells (cKit$^+$/Sca1$^+$/CD90.1$^{lo/-}$/Lin$^-$) are expressed as a percent of total bone marrow cells (M±SD, n=10, *P<0.05). B, The number of LT-HSCs (phenotypically defined as CD34$^-$Flk$_2$$^-$KTLS) were expressed as a percentage of total KTLS (M±SD, n=6, *P<0.05). C, Telomere length in KTLS cells from WT and ApoE$^{-/-}$ mice was expressed as relative telomere length (M±SD, n=8, *P<0.05). D, Side population cells (Hoechst^{low} KTLS) were detected in total KTLS cells from WT mice (18.8±4.4%) and ApoE$^{-/-}$ mice (6.2±1.7% *) expressed as a percent of total KTLS cells (n=5, *P<0.05). E, The percent of CD45.2$^+$ mononuclear cells in peripheral blood was determined 4, 8, and 12 weeks after transplantation (M±SD, n=6 to 7, **P<0.01 vs transplant with CD45.2 WT HSCs). F, The percent of CD45.2$^+$ populations in total KTLS cells 12 weeks after transplantation were measured in the recipients with KTLS cells from WT mice (51.4±6.2%) or with KTLS cells from ApoE$^{-/-}$ mice (20.3±9.5% *) (M±SD, n=6 to 7, *P<0.05 vs transplant with WT KTLS cells). KTLS indicates cKit$^+$/Sca1$^+$/CD90.1$^{lo/-}$/Lin$^-$; LT-HSC, long-term hematopoietic stem cell; WT, wild type.

Consistent with the reduced phenotypically defined LT-HSC population, the reconstitution capacity of KTLS cells from ApoE$^{-/-}$ and HCD mice was significantly impaired (Figure 1E). Similarly, CD45.2$^+$ population in total KTLS of the recipients transplanted with KTLS cells from ApoE$^{-/-}$ mice is significantly lower than those of the recipients transplanted with KTLS cells from WT mice 12 weeks after competitive transplantation (Figure 1F).

We also investigated the effects of hypercholesterolemia onto HSCs in high cholesterol diet (HCD) induced hypercholesterolemic model. KTLS population in HCD mice increased to 4-fold higher than WT mice fed with normal chow diet

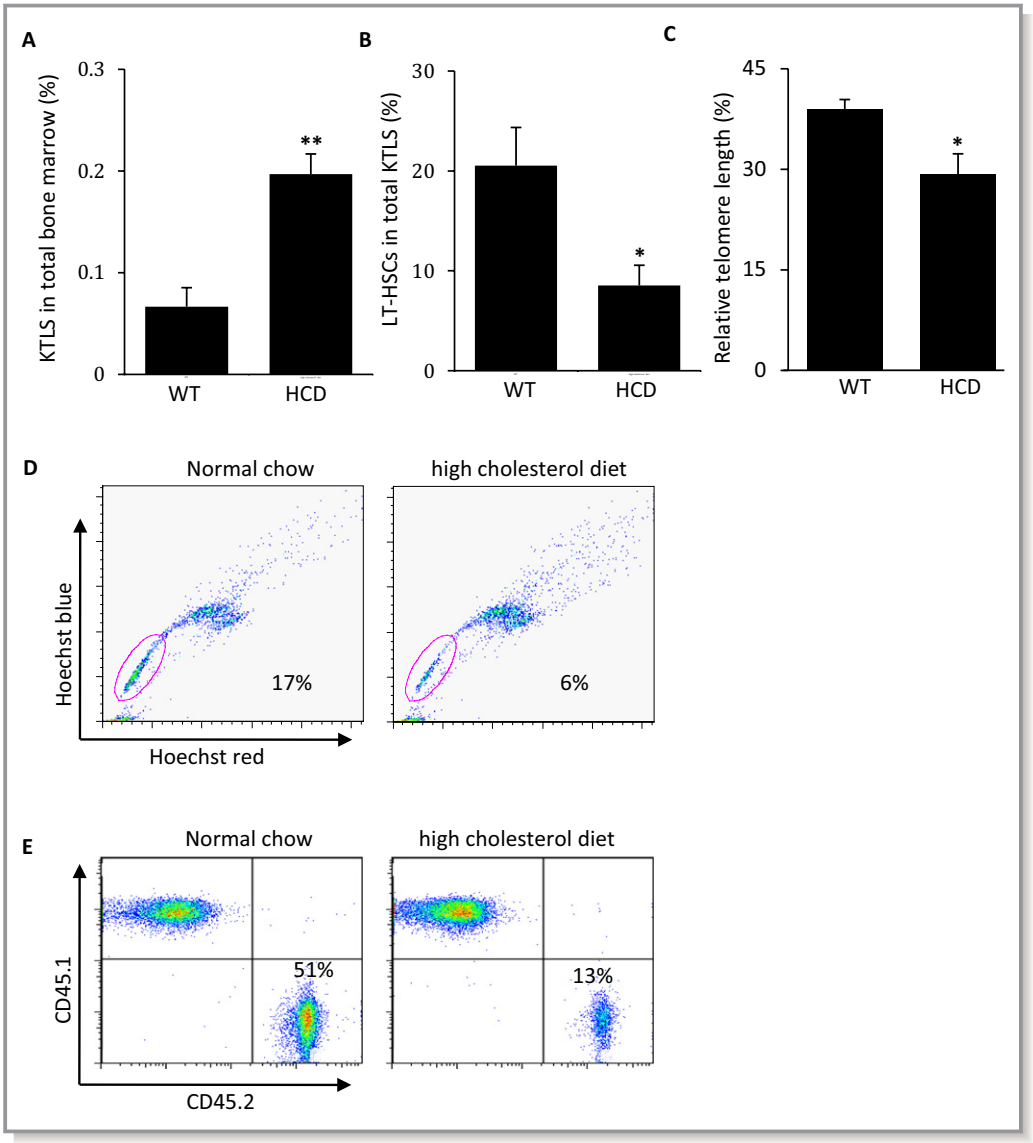

Figure 2. High cholesterol diet-induced hypercholesterolemia also accelerates the ageing of HSCs. A, KTLS were derived from WT mice or WT mice fed a high cholesterol diet (HCD). The number of KTLS cells is expressed as a percent of total bone marrow mononuclear cells (M±SD, n=15, ***P*<0.01). B, The number of phenotypically defined LT-HSCs ($CD34^-Flk_2^-$KTLS) in WT and HCD mice were expressed as a percent of total KTLS cells (M±SD, n=6, **P*<0.05 vs WT). C, Telomere length in KTLS cells from WT and HCD mice was expressed as relative telomere length (M±SD, n=8, **P*<0.05). D, Side population of KTLS cells in normal chow mice (16.5±2.1%) and HCD mice (5.2±3.8% *), determined by the phenotype $Hoechst^{low}$ KTLS, were expressed as a percent of total KTLS cells. The numbers indicate the M±SD (n=5, **P*<0.05 vs normal chow mice). E, The percent of $CD45.2^+$ populations in total KTLS cells 12 weeks after transplantation were measured in the recipients with KTLS cells from normal chow mice (50±3.2%) or with KTLS cells from HCD mice (15±11.5% *) (n=6, **P*<0.05 vs transplant with KTLS cells from normal chow mice). LT-HSC indicates long-term hematopoietic stem cell; WT, wild type.

(Figure 2A), while the ratio of phenotypically defined LT-HSCs in total KTLS population significantly decreased (Figure 2B). Telomere length was also significantly shorter than KTLS cells from WT mice on normal chow diet (Figure 2C). Side population of KTLS was 3-fold fewer than those in WT mice on normal chow diet (Figure 2D). A similar impairment of reconstitution capacity occurred after transplantation of KTLS cells from HCD mice (Figure 2E). The findings derived from high-cholesterol-diet-fed mice excluded the possibility that the deleterious effects of hypercholesterolemia on HSCs were due to loss of Apolipoprotein E expression. Taken together, these results indicate that hypercholesterolemia accelerates the ageing of HSCs manifested by loss of quiescence, expansion of the HSC compartment, and a decrease in their reconstitution capacity.

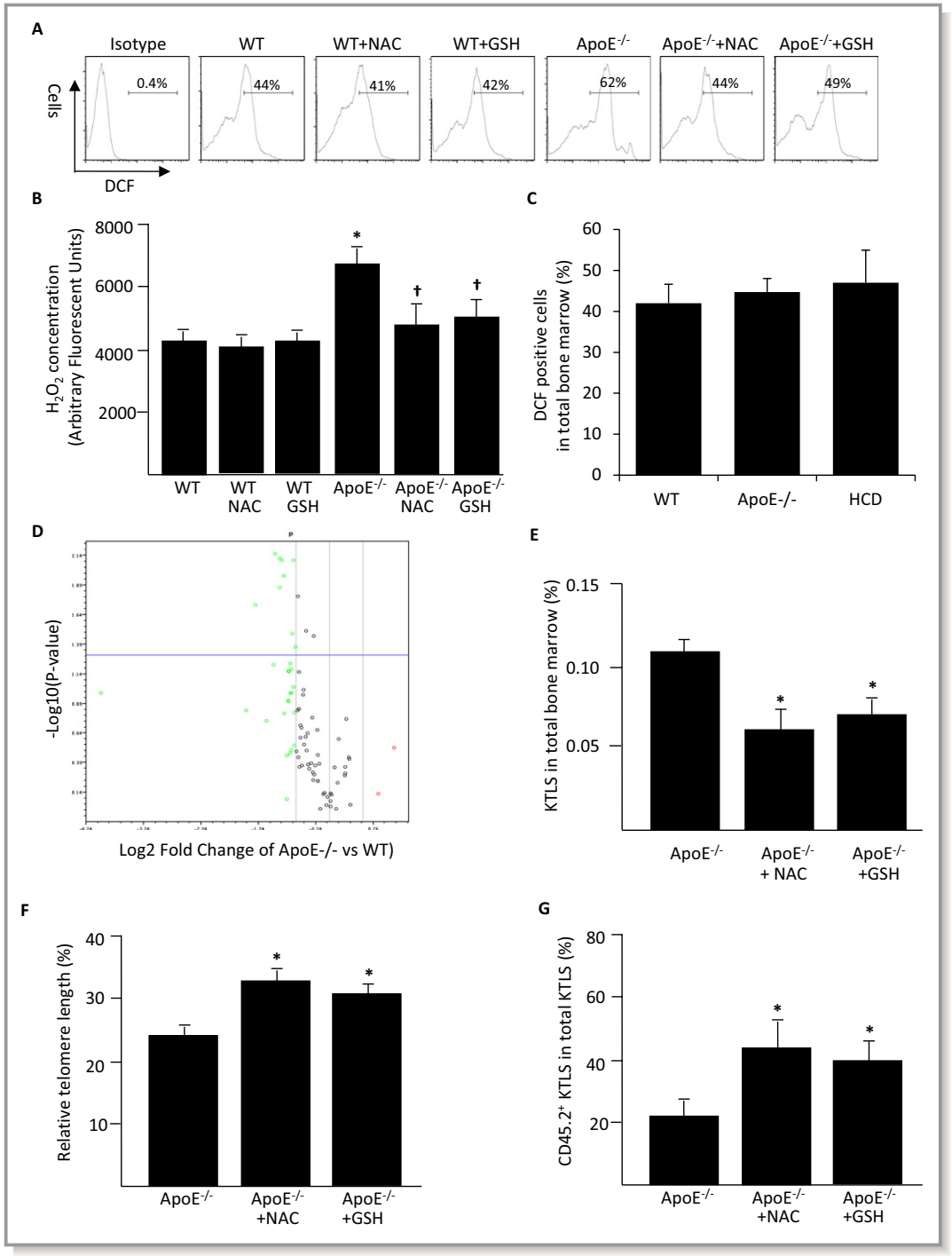

Figure 3. Hypercholesterolemia-induced ageing of HSCs is oxidant stress-dependent. A, ROS level was measured by DCF staining in KTLS cells from WT (46.1±5.3%), *N*-acetylcysteine (NAC)-treated WT (40.7±3.3%), GSH-treated WT (42.7±4.1%), ApoE$^{-/-}$ (60.5±4.8% *), NAC-treated ApoE$^{-/-}$ (42.6±5.3% †) and GSH-treated mice (49.4±2.5% †). The number represents the M±SD (n=8, *P<0.05 vs WT; †P<0.05 vs ApoE$^{-/-}$). B, H_2O_2 concentrations expressed as arbitrary fluorescent units in KTLS cells from WT, NAC-treated WT, GSH-treated WT, ApoE$^{-/-}$, NAC-treated ApoE$^{-/-}$ and GSH-treated mice (M±SD, n=6, *P<0.05; †P<0.05 vs ApoE$^{-/-}$). C, ROS level did not show difference between total bone marrow cells from WT, ApoE$^{-/-}$ and HCD mice. ROS level was detected by DCF staining and FACS (n=6). D, Gene expression profiling of oxidant stress responsive and antioxidant genes by PCR array. Log2 transformed gene expression values are shown for ApoE$^{-/-}$ vs WT HSCs. Circles show upregulated (red) and downregulated (green) genes. (n=3). E, The frequency of KTLS cells from ApoE$^{-/-}$, NAC-treated ApoE$^{-/-}$ and GSH-treated ApoE$^{-/-}$ mice expressed as a percent of total bone marrow cells (M±SD, n=8 to 10, *P<0.05 vs ApoE$^{-/-}$). F, Relative telomere length in KTLS cells from ApoE$^{-/-}$, NAC-treated ApoE$^{-/-}$ and GSH-treated ApoE$^{-/-}$ mice (M±SD, n=8, *P<0.05, vs ApoE$^{-/-}$). G, The percent of CD45.2^{+} KTLS cells 12 weeks after competitive transplantation (M±SD, n=6 to 7, *P<0.05 vs transplant with ApoE$^{-/-}$ KTLS). DCF indicates 2′,7′-Dichlorofluorescin diacetate; HCD, high cholesterol diet; FACS, flowcytometry; GSH, L-Glutamyl-L-Cysteinyl-Glycine; HSC, hematopoietic stem cell; PCR, polymerase chain reaction; ROS, reactive oxygen species; WT, wild type.

ROS Levels are Greater in HSCs From Hypercholesterolemic Mice

Oxidant stress has been suggested as a major factor that causes ageing and senescence of HSCs.[12,13] Therefore, we determined whether hypercholesterolemia induces oxidant stress in HSCs. Significantly higher reactive oxygen species (ROS) levels were shown in KTLS cells from ApoE$^{-/-}$ mice than WT mice by DCF staining (Figure 3A) and H_2O_2 assay (Figure 3B). DCF staining and flowcytometry showed that ROS levels in total bone marrow cells had no significant difference between WT, HCD mice and ApoE$^{-/-}$ mice (Figure 3C). Treatment of ApoE$^{-/-}$ mice with the antioxidant *N*-acetylcysteine (NAC) or GSH significantly reduced ROS levels within their KTLS cells (Figures 3A and 3B).

To gain insight into the basis for oxidant stress in HSCs from hypercholesterolemic mice, we profiled the expression of genes involved in antioxidant defense and ROS metabolism by RT-PCR (Table 2). The expression of antioxidant genes, including *Duox1*, *Sod1*, *Srxn1*, and *Prdx6-ps1* was paradoxically significantly lower in ApoE$^{-/-}$ KTLS cells (Figure 3D; Table 3). In addition, *Nox1*, which is involved in reactive oxygen species metabolism, was significantly downregulated in ApoE$^{-/-}$ KTLS cells.

Treatment with NAC or GSH reversed the oxidant-induced changes in the KTLS cells of ApoE$^{-/-}$ mice. KTLS frequency in the bone marrow of NAC- or GSH-treated ApoE$^{-/-}$ mice decreased to 0.07±0.01 or 0.08±0.01 respectively (Figure 3E). The mean relative telomere length of KTLS cells from NAC-or GSH-treated ApoE$^{-/-}$ mice increased by 18% or 14% respectively (Figure 3F). Finally, NAC and GSH significantly restored the reconstitution capacity of ApoE$^{-/-}$ KTLS cells to a level comparable to that in WT KTLS cells (Figure 3G). Consistent with the findings in ApoE$^{-/-}$ mice, KTLS cells from HCD mice also showed significantly greater ROS levels (Figure 4A) and nitrotyrosine accumulation than KTLS cells from WT mice (Figures 4B and 4C). These findings indicate that hypercholesterolemia induces oxidant stress in HSCs that causes accelerated ageing manifested by loss of quiescence, expansion of the HSC compartment, and impaired reconstitution capacity.

Oxidized low-density lipoprotein (oxLDL) accumulates and causes oxidant stress in a variety of cells and tissues. Oxidized-LDL has also been found in the peripheral blood cells of mouse models of hypercholesterolemia.[14] In our study, KTLS cells from ApoE$^{-/-}$ mice showed accumulation of oxLDL but none was found in those from WT mice (Figure 5A). We screened for the expression of major oxLDL receptors, including scavenger receptors A1/A2 (SRA1, A2), scavenger receptors B1/B2 (SRB1, B2), CD36, CD68, and lectin-like oxidized low-density lipoprotein receptor 1 (LOX-1) in KTLS from WT and ApoE$^{-/-}$ mice. SRB2 and LOX-1 were detected

Table 2. Gene Expression Profiling in HSC From ApoE$^{-/-}$ and Wild Type Mice Using the Mouse Oxidative Stress and Antioxidant Defense PCR Array

Gene	Description	Fold Difference	*P* Value
Antioxidants			
Glutathione Peroxidases			
Gpx1	Glutathione peroxidase 1	−1.0081	0.956027
Gpx2	Glutathione peroxidase 2	−1.3394	0.475966
Gpx3	Glutathione peroxidase 3	1.083	0.684087
Gpx4	Glutathione peroxidase 4	−1.2099	0.522119
Gpx5	Glutathione peroxidase 5	ND	
Gpx6	Glutathione peroxidase 6	ND	
Gpx7	Glutathione peroxidase 7	ND	
Gpx8	Glutathione peroxidase 8 (putative)	−1.4793	0.323662
Gstk1	Glutathione S-transferase kappa 1	−1.4759	0.087374
Peroxiredoxins			
Ehd2	EH-domain containing 2	−1.273	0.413764
Prdx1	Peroxiredoxin 1	−1.1741	0.340709
Prdx2	Peroxiredoxin 2	−1.2468	0.512938
Prdx3	Peroxiredoxin 3	1.2585	0.982695
Prdx4	Peroxiredoxin 4	−1.3271	0.206431
Prdx5	Peroxiredoxin 5	1.1852	0.518617
Prdx6	Peroxiredoxin 6	−1.6798	0.054079
Other Peroxidases			
Aass	Aminoadipate-semialdehyde synthase	ND	
Apc	Adenomatosis polyposis coli	−1.5564	0.298982
Cat	Catalase	−1.2268	0.565475
Ctsb	Cathepsin B	−1.3179	0.451701
Duox1	Dual oxidase 1	−2.0022	0.046937
Epx	Eosinophil peroxidase	2.1412	0.337539
Kif9	Kinesin family member 9	−1.6682	0.123693
Lpo	Lactoperoxidase	−1.4158	0.422905
Mpo	Myeloperoxidase	1.0607	0.973049
Prdx6-ps1	Peroxiredoxin 6, pseudogene 1	−1.4896	0.027915
Ptgs1	Prostaglandin-endoperoxide synthase 1	−1.2325	0.203506
Ptgs2	Prostaglandin-endoperoxide synthase 2	−1.7032	0.909401
Rag2	Recombination activating gene 2	−1.6113	0.328386
Serpinb1b	Serine (or cysteine) peptidase inhibitor, clade B, member 1b	1.2441	0.46979

Continued

Table 2. Continued

Gene	Description	Fold Difference	*P* Value
Slc41a3	Solute carrier family 41, member 3	−1.3028	0.514791
Tmod1	Tropomodulin 1	−1.0057	0.713136
Tpo	Thyroid peroxidase	ND	
Other Antioxidants			
Gsr	Glutathione reductase	1.177	0.570362
Nxn	Nucleoredoxin	−1.5139	0.297957
Sod1	Superoxide dismutase 1, soluble	−1.3898	0.04285
Sod3	Superoxide dismutase 3, extracellular	ND	
Srxn1	Sulfiredoxin 1 homolog (*S. cerevisiae*)	−1.8552	0.031105
Txnrd1	Thioredoxin reductase 1	1.2383	0.440955
Txnrd2	Thioredoxin reductase 2	−1.5386	0.124392
Txnrd3	Thioredoxin reductase 3	−1.6188	0.092817
Zmynd17	Zinc finger, MYND domain containing 17	−1.7592	0.176509
Genes Involved in Reactive Oxygen Species (ROS) Metabolism			
Superoxide Dismutases			
Sod1	Superoxide dismutase 1, soluble	−1.3898	0.04285
Sod2	Superoxide dismutase 2, mitochondrial	−1.7032	0.335827
Sod3	Superoxide dismutase 3, extracellular	ND	
Other Genes Involved in Superoxide Metabolism			
Ccs	Copper chaperone for superoxide dismutase	−2.1859	0.161437
Cyba	Cytochrome b-245, alpha polypeptide	−1.0557	0.912461
Ncf2	Neutrophil cytosolic factor 2	−1.098	0.823474
Nox1	NADPH oxidase 1	−2.4994	0.014198
Nox4	NADPH oxidase 4	ND	
Noxa1	NADPH oxidase activator 1	ND	
Noxo1	NADPH oxidase organizer 1	−1.5965	0.053112
Recql4	RecQ protein-like 4	−1.3612	0.230672
Scd1	Stearoyl-Coenzyme A desaturase 1	−1.1368	0.951845
Other Genes Involved in ROS Metabolism			
Fmo2	Flavin containing monooxygenase 2	ND	
Il19	Interleukin 19	−1.4455	0.221795
Il22	Interleukin 22	ND	

Continued

Table 2. Continued

Gene	Description	Fold Difference	*P* Value
Oxidative Stress Response Genes			
Aass	Aminoadipate-semialdehyde synthase	ND	
Als2	Amyotrophic lateral sclerosis 2 (juvenile) homolog (human)	−1.961	0.016499
Apoe	Apolipoprotein E	−16.129	0.103123
Cat	Catalase	−1.2268	0.565475
Ctsb	Cathepsin B	−1.3179	0.451701
Duox1	Dual oxidase 1	−2.0022	0.046937
Epx	Eosinophil peroxidase	2.1412	0.337539
Ercc2	Excision repair cross-complementing rodent repair deficiency, complementation group 2	−1.4422	0.193837
Ercc6	Excision repair cross-complementing rodent repair deficiency, complementation group 6	−1.649	0.332206
Gab1	Growth factor receptor bound protein 2-associated protein 1	−1.5745	0.203367
Gpx1	Glutathione peroxidase 1	−1.0081	0.956027
Gpx2	Glutathione peroxidase 2	−1.3394	0.475966
Gpx3	Glutathione peroxidase 3	1.083	0.684087
Gpx4	Glutathione peroxidase 4	−1.2099	0.522119
Gpx5	Glutathione peroxidase 5	ND	
Gpx6	Glutathione peroxidase 6	ND	
Gpx7	Glutathione peroxidase 7	ND	
Idh1	Isocitrate dehydrogenase 1 (NADP+), soluble	1.2017	0.275654
Mpo	Myeloperoxidase	1.0607	0.973049
Mpp4	Membrane protein, palmitoylated 4 (MAGUK p55 subfamily member 4)	ND	
Nqo1	NAD(P)H dehydrogenase, quinone 1	−1.4289	0.289926
Nudt15	Nudix (nucleoside diphosphate linked moiety X)-type motif 15	−1.4965	0.179943
Park7	Parkinson disease (autosomal recessive, early onset) 7	−1.3995	0.111426
Ppp1r15b	Protein phosphatase 1, regulatory (inhibitor) subunit 15b	−1.4759	0.152001
Prdx1	Peroxiredoxin 1	−1.1741	0.340709
Prdx2	Peroxiredoxin 2	−1.2468	0.512938

Continued

Table 2. Continued

Gene	Description	Fold Difference	*P* Value
Prdx6	Peroxiredoxin 6	−1.6798	0.054079
Prnp	Prion protein	−1.1768	0.645033
Psmb5	Proteasome (prosome, macropain) subunit, beta type 5	−1.3487	0.017754
Sod1	Superoxide dismutase 1, soluble	−1.3898	0.04285
Tpo	Thyroid peroxidase	ND	
Txnip	Thioredoxin interacting protein	−1.3866	0.305166
Txnrd2	Thioredoxin reductase 2	−1.5386	0.124392
Ucp3	Uncoupling protein 3 (mitochondrial, proton carrier)	−1.6798	0.046104
Xpa	Xeroderma pigmentosum, complementation group A	−1.6301	0.096519
Oxygen Transporters			
Aqr	Aquarius	−1.15	0.477341
Atr	Ataxia telangiectasia and rad3 related	−2.7861	0.142442
Cygb	Cytoglobin	−1.4623	0.588178
Dnm2	Dynamin 2	−1.6376	0.128693
Fancc	Fanconi anemia, complementation group C	−1.5709	0.045333
Hbq1a	Hemoglobin, theta 1A	1.1906	0.502386
Ift172	Intraflagellar transport 172 homolog (Chlamydomonas)	−1.6188	0.089111
Mb	Myoglobin	ND	
Ngb	Neuroglobin	ND	
Slc38a1	Solute carrier family 38, member 1	−1.1823	0.41057
Vim	Vimentin	−1.1741	0.595145
Xirp1	Xin actin-binding repeat containing 1	ND	

HSC indicates hematopoietic stem cell; PCR, polymerase chain reaction.

by RT-PCR and FACS (Figures 5B through 5E). The expression of SRB2 and LOX-1 was significantly lower in KTLS cells than in other bone marrow cells (Figures 5B through 5E). The expression of LOX-1 in KTLS cells from ApoE$^{-/-}$ mice significantly greater than those in KTLS cells from WT mice (Figures 5F and 5G). To verify the role of SRB2 and LOX-1 in the uptake of oxLDL, we inhibited the expression of SRB2 and LOX-1 by Lentivirus mediated shRNA against SRB2 or LOX-1 (Figures 5H and 5I). The inhibition of SRB2 or LOX-1 both significantly decreased the uptake of oxLDL by KTLS cells in vitro, while simultaneous inhibition of SRB2 and LOX-1 caused a synergystic decrease in the uptake of oxLDL (Figure 5J). These findings indicated that HSCs take up oxLDL by a

Table 3. Summary of Gene Expression Results Profiling of HSCs From ApoE$^{-/-}$ Versus WT Mice for Antioxidant and Oxidant Stress Responsive Genes by PCR Array

Gene	Description	Fold Difference	*P* Value
Als2	Amyotrophic lateral sclerosis 2 (juvenile) homolog (human)	−1.96	0.016
Duox1	Dual oxidase 1	−2.00	0.047
Fancc	Fanconi anemia, complementation group C	−1.57	0.045
Nox1	NADPH oxidase 1	−2.50	0.014
Prdx6-ps1	Peroxiredoxin 6, pseudogene 1	−1.49	0.028
Psmb5	Proteasome (prosome, macropain) subunit, beta type 5	−1.35	0.018
Sod1	Superoxide dismutase 1, soluble	−1.39	0.043
Srxn1	Sulfiredoxin 1 homolog (*S. cerevisiae*)	−1.86	0.031

HSCs indicates hematopoietic stem cells; PCR, polymerase chain reaction; WT, wild type.

receptor-mediated mechanism. Exposure of WT KTLS cells to oxLDL in vitro significantly increased oxidant stress (Figure 6A), decreased phenotypically defined LT-HSC population (Figure 6B), and reduced their reconstitution capacity in a concentration-dependent manner (Figure 6C). All these findings indicate that intracellular accumulation of oxLDL causes oxidant stress and accelerates ageing in HSCs of hypercholesterolemic mice.

In the previous studies, other mouse models of hypercholesterolemia have been used to investigate the effects of hypercholesterolemia onto HSCs, including ABCA1$^{-/-}$ ABCG1$^{-/-}$ or ApoE$^{-/-}$ mice fed on high-fat diet (HFD).[10,11] To further address the deleterious effects of hypercholesterolemia on HSCs, we reproduced the conditions of these studies by feeding ApoE$^{-/-}$ mice the same HFD used in these studies. The frequency of KTLS cells in these mice was 0.2% of total bone marrow cells, significantly higher than that in ApoE$^{-/-}$ mice on normal chow (Figure 7A). Consistent with this further expansion of KTLS compartment of Apo E$^{-/-}$ fed by HFD, DCF staining showed higher oxidant accumulation in KTLS cells as well (Figure 7B). More importantly, the HFD also induced a very significant monocytosis (Figures 8A through 8D) and >2-fold increase of spleen size (Figure 8E). Additionally, we measured serum cholesterol levels in ApoE$^{-/-}$ mice fed this specific HFD. The total serum cholesterol levels were exceedingly high, close to 1000 mg/dL (Figure 8F) which is comparable to the reported in the previous studies.[9]

ROS Triggers Ageing Related Signaling Pathways in HSCs From ApoE$^{-/-}$ Mice

We detected the phosphorylation of p38 MAPK in KTLS cells from WT and hypercholesterolemic mice. FACS analysis

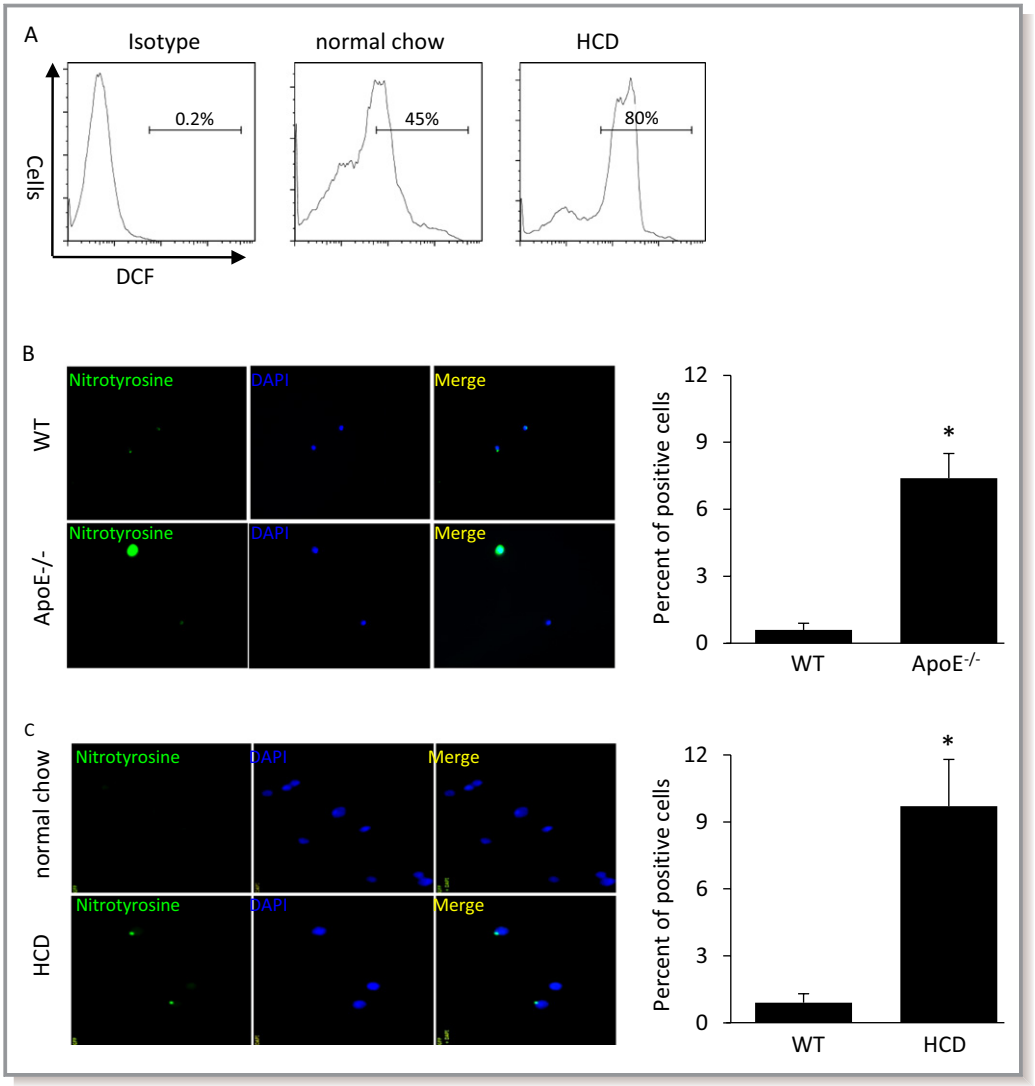

Figure 4. ROS level increases in KTLS cells isolated from HCD induced hypercholesterolemic mice. A, ROS level was measured by DCF staining in KTLS cells from WT mice (43±6.3%) and HCD mice (79±4.8% *). The number represents the M±SD (n=8, *P<0.05 vs normal chow). B and C, The accumulation of nitrotyrosine in KTLS cells from ApoE$^{-/-}$ mice (B) (n=6, *P<0.05 vs WT) or HCD mice (C) (n=6, *P<0.05 vs normal chow) was shown by. The number represents the M±SD. HCD indicates high cholesterol diet; ROS, reactive oxygen species; WT, wild type.

showed that phosphorylation of p38 MAPK was greater in KTLS cells from ApoE$^{-/-}$ mice, while the expression of total p38 showed no difference (Figure 9A). The phosphorylation of p38 MAPK in KTLS cells from ApoE$^{-/-}$ mice was further measured by Western blotting (Figures 9B and 9C). NAC treatment restored the phosphorylation of p38 MAPK in ApoE$^{-/-}$ mice (Figures 9A through 9C). In ApoE$^{-/-}$ mice, phosphorylation of p38 was greater in phenotypically defined LT-HSC than in short-term HSCs (ST-HSCs, phenotypically defined as CD34^{+}Flk$_2$$^{-}$KTLS), Lin^{-} and Lin^{+} bone marrow cells. It was greater in ST-HSC than in Lin^{-} and Lin^{+} bone marrow cells (Figure 9D). FACS analysis also showed greater phosphorylation of p38 MAPK in KTLS from HCD mice (Figure 9E). Treatment with p38 inhibitor SB203580 significantly increased the proportion of phenotypically defined LT-HSCs in ApoE$^{-/-}$ mice, but had no effect on the proportion of phenotypically defined LT-HSCs from WT mice (Figures 9F and 9G). Moreover, inhibition of p38 improved the reconstitution capacity of KTLS cells from ApoE$^{-/-}$ mice; whereas MEK1 inhibitor PD98059 had no effect on reconstitution capacity (Figure 9H). The findings suggested that the effect of hypercholesterolemia-induced oxidant stress on HSC ageing is mediated via activation of p38 MAPK.

To identify the molecular mechanisms that underlie the accelerated ageing of HSCs from hypercholesterolemic mice, we screened HSC genomic expression by microarrays which showed that of the genes that were differentially expressed, 398 genes were upregulated and 173 were downregulated

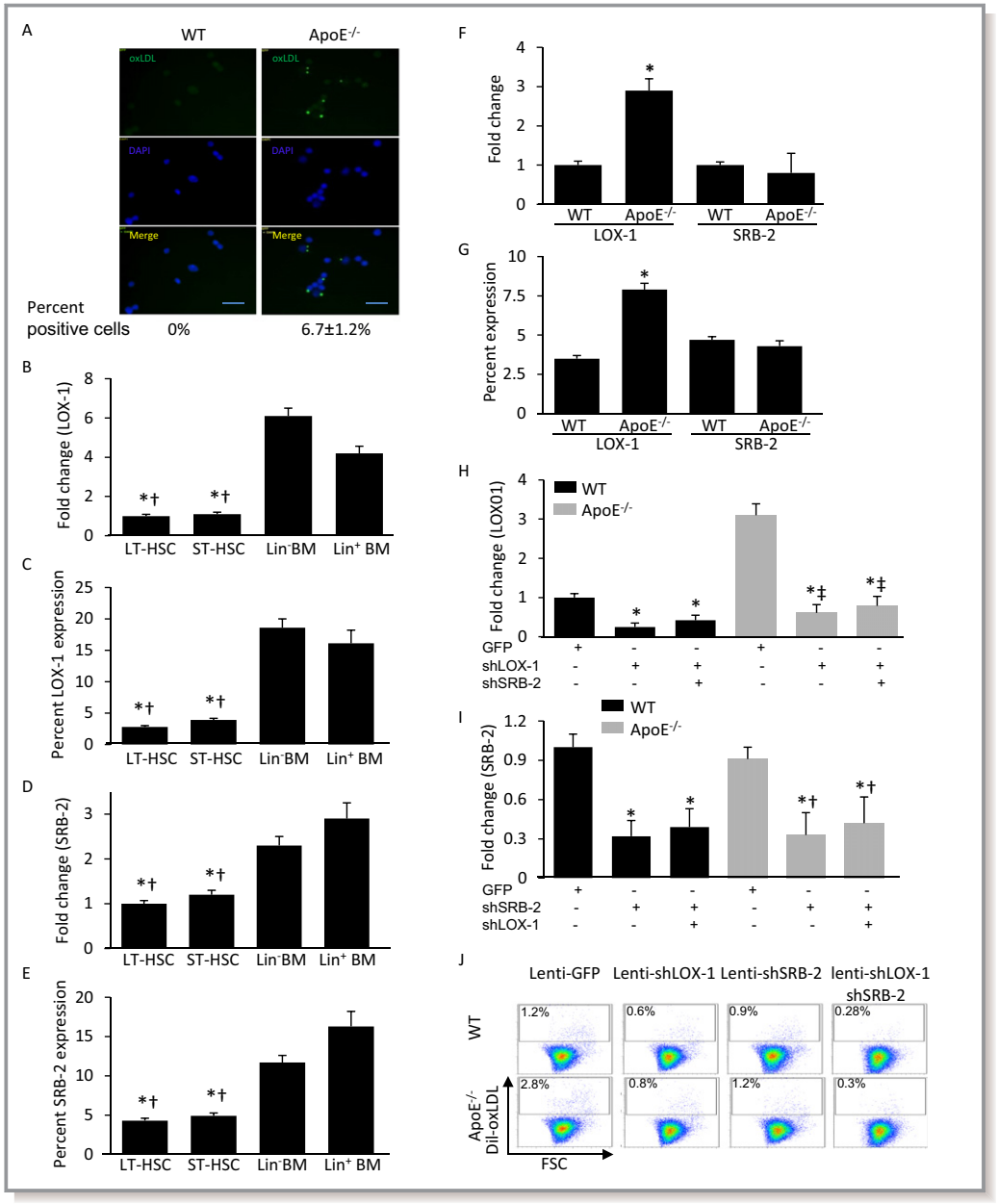

Figure 5. LOX-1 and SRB-2 mediates oxLDL uptake in KTLS cells. A, Accumulation of oxLDL in KTLS from ApoE$^{-/-}$ mice was shown by immunostaining (Bars, 50 μm). The number represents the M±SD (n=6, *P<0.05 vs WT mice). B and C, LOX-1 expression was detected by qRT-PCR (B) and flowcytometry (C) in CD34$^-$Flk$_2^-$KTLS cells, CD34$^+$Flk$_2^-$KTLS cells (phenotypically defined short term HSCs), Lin$^-$ bone marrow and Lin$^+$ marrow cells from WT mice. LOX-1 expression in the KTLS population was significantly lower than Lin$^-$ and Lin$^+$ bone marrow cells (M±SD, n=5, *P<0.05, vs Lin+ bone marrow cells; †P<0.05, vs total bone marrow cells). D and E, SRB-2 expression was detected by qRT-PCR (D) and Flowcytometry (E) in CD34$^-$Flk$_2^-$, CD34$^+$Flk$_2^-$KTLS cells, Lin$^-$ and Lin$^+$ marrow cells from ApoE$^{-/-}$ mice. LOX-1 expression in the KTLS population was significantly lower than Lin$^-$ and Lin$^+$ marrow cells (M±SD, n=5, *P<0.05, vs Lin$^-$ bone marrow cells; †P<0.05, vs Lin$^+$ bone marrow cells). F and G, The expression of LOX-1 in KTLS cells isolated from ApoE$^{-/-}$ mice was significantly greater than those in KTLS cells isolated from WT mice. No difference was detected in the expression of SRB-2. The expression of LOX-1 and SRB-2 was measured by qRT-PCR (F) and flowcytometry (G) (M±SD, n=5,*P<0.05, vs WT KTLS). H and I, The expression of LOX-1 and SRB-2 in KTLS cells from WT and ApoE$^{-/-}$ mice after transfection of Lenti-shLOX-1 or Lenti-shSRB-2 was detected by qRT-PCR (H) and flowcytometry (I) (M±SD, n=6,*P<0.05, vs WT KTLS transfected with Lenti-GFP; †P<0.05, ‡P<0.01, vs ApoE$^{-/-}$ KTLS transfected with Lenti-GFP). J, in vitro oxLDL uptake was measured by Flowcytometry in Lenti-GFP WT KTLS (1.26±0.1%), Lenti-shLOX-1 WT KTLS (0.65±0.1% *), Lenti-shSRB-2 WT KTLS (0.91±0.1% *), Lenti-shLOX-1/SRB-2 WT KTLS (0.28±0.1% *), Lenti-GFP ApoE$^{-/-}$ KTLS (2.92±0.1%), Lenti-shLOX-1 ApoE$^{-/-}$ KTLS (0.79±0.1% †), Lenti-shSRB-2 ApoE$^{-/-}$ KTLS (1.21±0.1% †) and Lenti-shLOX-1/SRB-2 ApoE$^{-/-}$ KTLS (0.33±0.1% ‡). The number represents the M±SD (n=8,*P<0.05, vs Lenti-GFP WT KTLS; †P<0.05, ‡P<0.01, vs Lenti-GFP ApoE$^{-/-}$ KTLS). BM indicates bone marrow; FSC, forward side scatter; GFP, green fluorescent protein; LOX-1, lectin-like oxidized low-density lipoprotein receptor 1; LT-HSC, long-term hematopoietic stem cell; MAPK, mitogen activated protein kinase; oxLDL, oxidized low-density lipoprotein; qRT-PCR, quantitative reverse transcription polymerase chain reaction; SRB-2, scavenger receptors B2; ST-HSC, short term hematopoietic stem cell; WT, wild type.

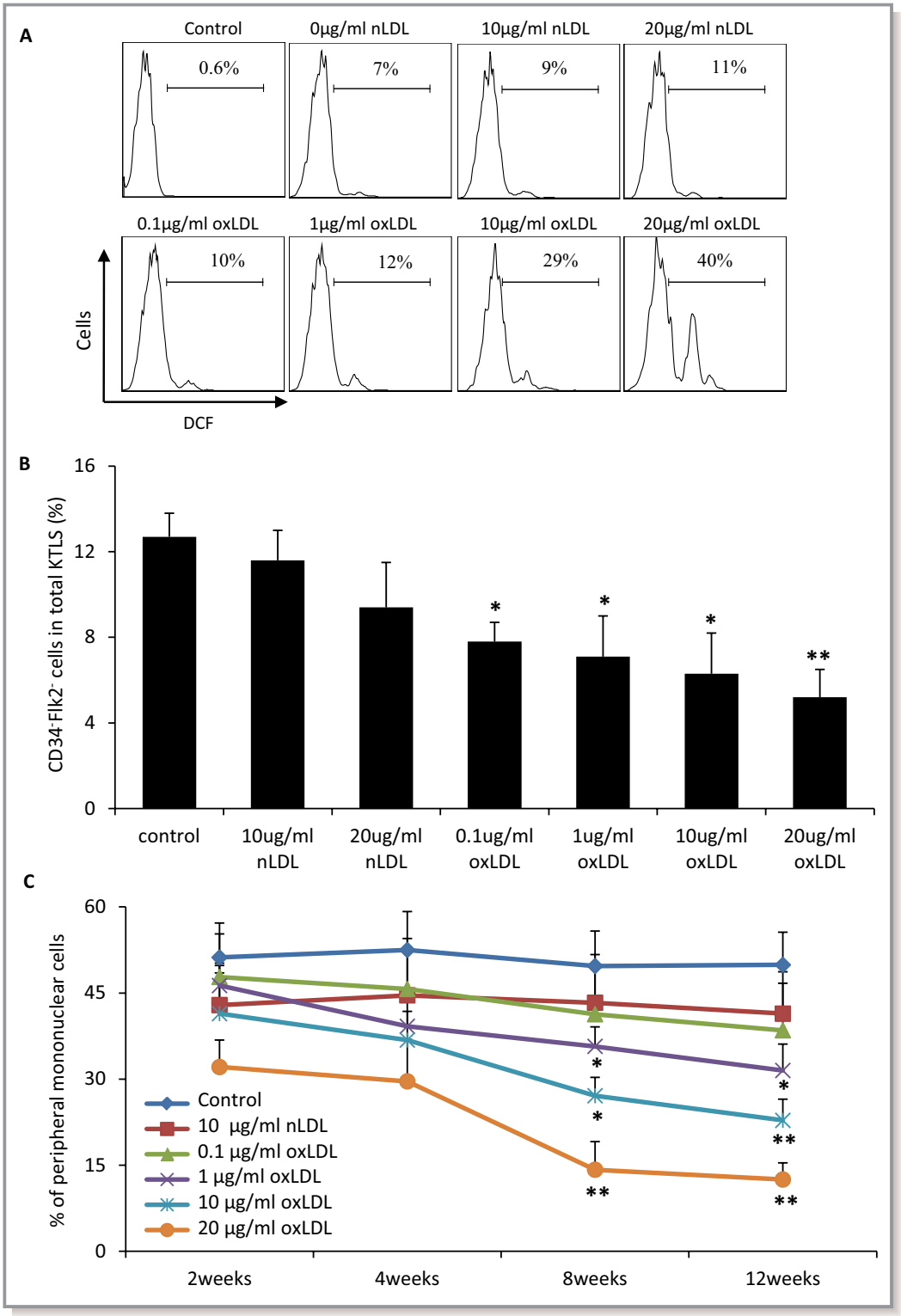

Figure 6. Accumulation of oxLDL causes oxidant stress, decreases LT-HSC compartment and impairs reconstitution capacity of KTLS cells. A, ROS level was measured by DCF staining in WT KTLS cells treated with 0 μg/mL nLDL (7.5±0.9%), 10 μg/mL nLDL (8.7±1.2%), 20 μg/mL nLDL (11.6±1.7%), 0.1 μg/mL oxLDL (9.8±0.6%), 1 μg/mL oxLDL (11.7±1.6%), 10 μg/mL oxLDL (28.5±.4% *) and 20 μg/mL oxLDL (39.8±5.7% **). The numbers represent M±SD (n=8, *P<0.05, **P<0.01 vs 0 μg/mL nLDL group). B, Phenotypically defined LT-HSC population of WT KTLS cells in vitro culture was measured by Flowcytometry. The number of LT-HSC was represented as percent of total KTLS cells (M±SD, n=8, *P<0.05, **P<0.01, vs control). C, Competitive HSC transplantation assay of WT KTLS cells treated with oxLDL. The percent of $CD45.2^+$ cells in peripheral blood were represented as M±SD (n=8, *P<0.05, **P<0.01, vs control). LT-HSC indicates long-term hematopoietic stem cell; oxLDL, oxidized low-density lipoprotein; ROS, reactive oxygen species; WT, wild type.

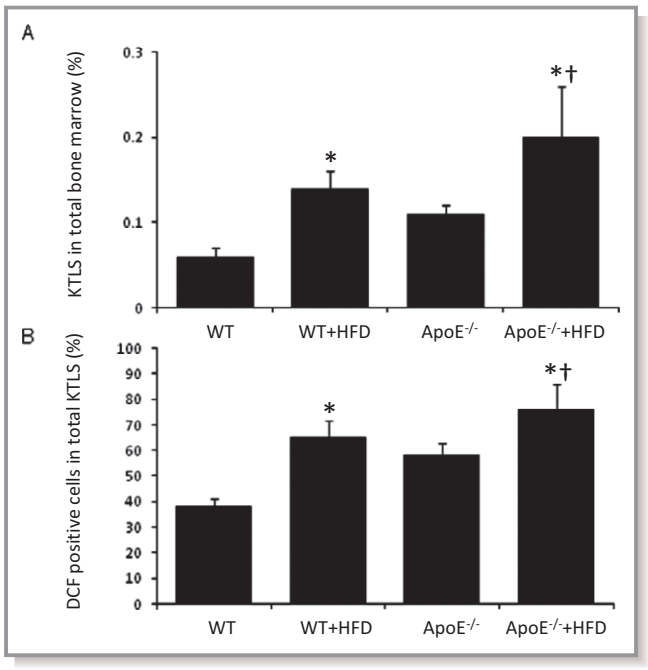

Figure 7. High fat diet further increased expansion and ROS level in HSC compartment of ApoE$^{-/-}$ mice. A, The frequency of KTLS cells are expressed as a percent of total bone marrow mononuclear cells (M±SD, n=15, *P<0.05 vs normal chow mice; †P<0.01 vs ApoE$^{-/-}$ mice). B, ROS level was detected by DCF staining and Flowcytometry in KTLS cells. The number within each histogram represents the M±SD (n=8, *P<0.05 vs normal chow mice, †P<0.05 vs ApoE$^{-/-}$ mice). HFD indicates high fat diet; HSC, hematopoietic stem cell; ROS, reactive oxygen species; WT, wild type.

(Figure 10A). These candidate genes were further evaluated by Ingenuity Pathways Analysis. Four significant canonical pathways were identified: p53 signaling; G_2/M DNA damage checkpoint regulation; IL-8 signaling; and one carbon pool by folate (Figure 10B). These pathways all involve cell cycle regulation. The Cip/Kip family of CDK inhibitors was consistently represented in each pathway. Ingenuity Pathways Analysis indicated high Notch1 activity in KTLS cells from ApoE$^{-/-}$ mice (Figure 10C).

Besides the Cip/Kip family, the Ink4 family also responds to increased ROS and regulates HSC function.[11] Expression of $p19^{Arf}$, $p21^{Waf1}$, and $p27^{Kip1}$ were significantly increased in KTLS cells from ApoE$^{-/-}$ mice, which was reversed by NAC or SB203580 treatment, but not by treatment with PD98059 (Figure 11A). The expressions of $p19^{Arf}$, $p21^{Waf1}$, and $p27^{Kip1}$ were higher in phenotypically defined LT-HSCs than in ST-HSCs from ApoE$^{-/-}$ mice (Figure 11B). To identify the role of $p19^{Arf}$, $p21^{Waf1}$, and $p27^{Kip1}$ in the deleterious effects induced by hypercholesterolemia, we inhibited their expression in KTLS cells from WT and ApoE$^{-/-}$ mice by Lentivirus mediated shRNA transfection. The positive cells were labeled by GFP and purified by FACS sorting. RT-PCR showed that the expression of $p19^{Arf}$, $p21^{Waf1}$, and $p27^{Kip1}$ was effectively inhibited in KTLS cells from WT and ApoE$^{-/-}$ mice (Figures 12A through 12C). FACS analysis showed that inhibition of $p19^{Arf}$, $p21^{Waf1}$, and $p27^{Kip1}$ significantly increased CD34^{-}Flk$_2^{-}$ populations of KTLS cells two weeks after shRNA transfection (Figure 12D). We measured the proliferation of KTLS cells in vitro by Ki67 staining and FACS analysis. The inhibition of $p19^{Arf}$, $p21^{Waf1}$, and $p27^{Kip1}$ increased the proliferation in CD34^{-}Flk$_2^{-}$ populations (Figure 12E), but decreased the proliferation in CD34^{+}Flk$_2^{-}$ populations (Figure 12F). FACS analysis for Annexin V staining showed that the inhibition of $p19^{Arf}$ and $p21^{Waf1}$ significantly increased apoptosis in both CD34^{-}Flk$_2^{-}$ and CD34^{+}Flk$_2^{-}$ populations (Figures 12G and 12H), while no difference was found in the $p27^{Kip1}$ inhibited groups. These findings indicate that the activation of the critical cell cycle regulators, $p19^{Arf}$, $p21^{Waf1}$, and $p27^{Kip1}$ contribute in the regulation of KTLS expansion and phenotypically defined LT-HSC decrease in hypercholesterolemic mice.

Notch1 Expression is Greater in HSCs From Hypercholesterolemic Mice

Ingenuity Pathway Analysis also suggested that Notch signaling might be increased in HSCs isolated from hypercholesterolemic mice (Figure 10C). RT-PCR confirmed that the expression of Notch1 was greater in HSCs from hypercholesterolemic mice (Figure 13A). Further, Notch1 expression was significantly greater in phenotypically defined ST-HSCs than LT-HSCs in WT and ApoE$^{-/-}$ mice; however, Notch1 expression in ApoE$^{-/-}$ ST-HSCs was significantly greater than that in WT ST-HSC (Figure 13B). Treatment of hypercholesterolemic mice with antioxidant NAC or p38 inhibitor SB203580 significantly reduced the expression of Notch1 in HSC from ApoE$^{-/-}$ mice (Figures 13A and 13C). The treatment of WT KTLS cells in vitro with SB203580 also decreased Notch1 expression in a concentration-dependent manner (Figure 13D). The inhibition of p38 also upregulated the expression of Sirt1, which has been shown to reduce Notch activity by cleaving Notch intracellular domain. MG132, an inhibitor of Sirt1, reversed the decrease of the Notch intracellular domain caused by SB203580 treatment (Figure 13E). These findings indicate that the ROS-p38 axis augments Notch1 activity in HSCs of hypercholesterolemic mice. Treatment of hypercholesterolemic mice in vivo with the γ-secretase inhibitor, DAPT, significantly decreased the size of KTLS compartment and increased the number of phenotypically defined LT-HSCs, while in vitro treatment of KTLS cells with DAPT significantly decreased proliferation (Figures 13F and 13G). The findings are supported by a previous study.[15] Together, these results indicate that the ROS-p38-induced increase of Notch1 activity drives the expansion of HSC compartment in hypercholesterolemic mice.

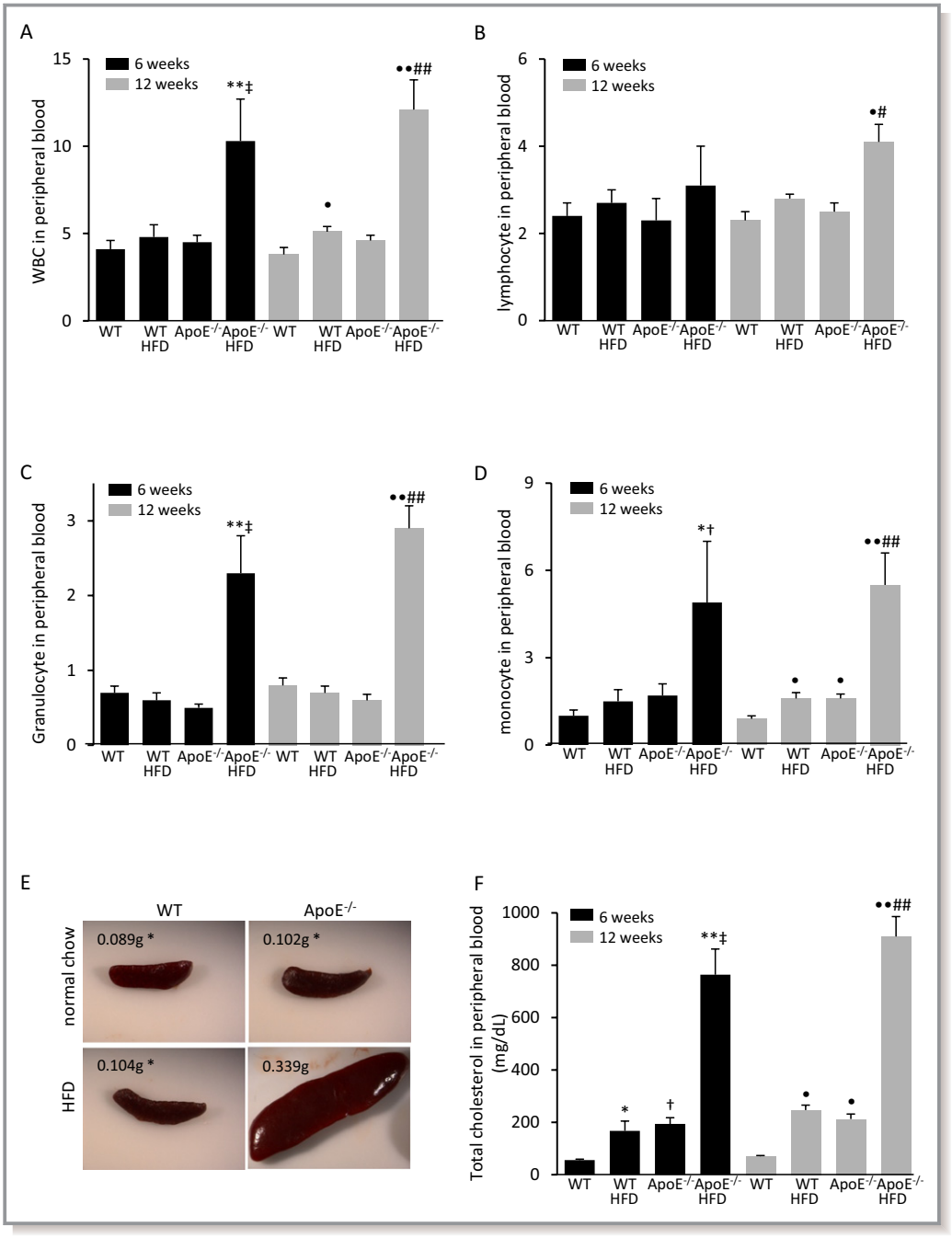

Figure 8. High fat diet induced monocytosis and spleen hypertrophy in ApoE$^{-/-}$ mice. A through D, White blood cells (A), lymphocytes (B), granulocytes (C) and monocytes (D) in peripheral blood of WT, HFD+WT, ApoE$^{-/-}$ and HFD ApoE$^{-/-}$ mice at 6 and 12 weeks after HFD feeding (n=6, *P<0.05,**P<0.01 vs WT 6 weeks; $^{\dagger}P$<0.05, $^{\ddagger}P$<0.01 vs ApoE$^{-/-}$ 6 weeks; •P<0.05, ••P<0.01 vs WT 12 weeks; $^{\#}P$<0.05, $^{\#\#}P$<0.01 vs ApoE$^{-/-}$ 12 weeks). E, The spleen weight 12 weeks after HCD feeding (n=6, *P<0.05, vs HFD fed ApoE$^{-/-}$ mice). F, Cholesterol level in peripheral blood was measured at 6 and 12 weeks after HFD feeding (n=6, *P<0.05,**P<0.01 vs WT 6 weeks; $^{\dagger}P$<0.05, $^{\ddagger}P$<0.01 vs ApoE$^{-/-}$ 6 weeks; •P<0.05, ••P<0.01 vs WT 12 weeks; #P<0.05, ##P<0.01 vs ApoE$^{-/-}$ 12 weeks). HCD indicates high cholesterol diet; HFD, high fat diet; WBC, white blood cells; WT, wild type.

Discussion

Throughout the lifespan of an organism, HSCs supply the entire array of hematopoietic cell lineages, which are necessary for survival. HSCs exert their essential function via their capacities of pluripotency and self-renewal.[15] To maintain these capacities and thus protect against exhaustion of the HSC population, most HSCs are kept in a state of quiescence and only a

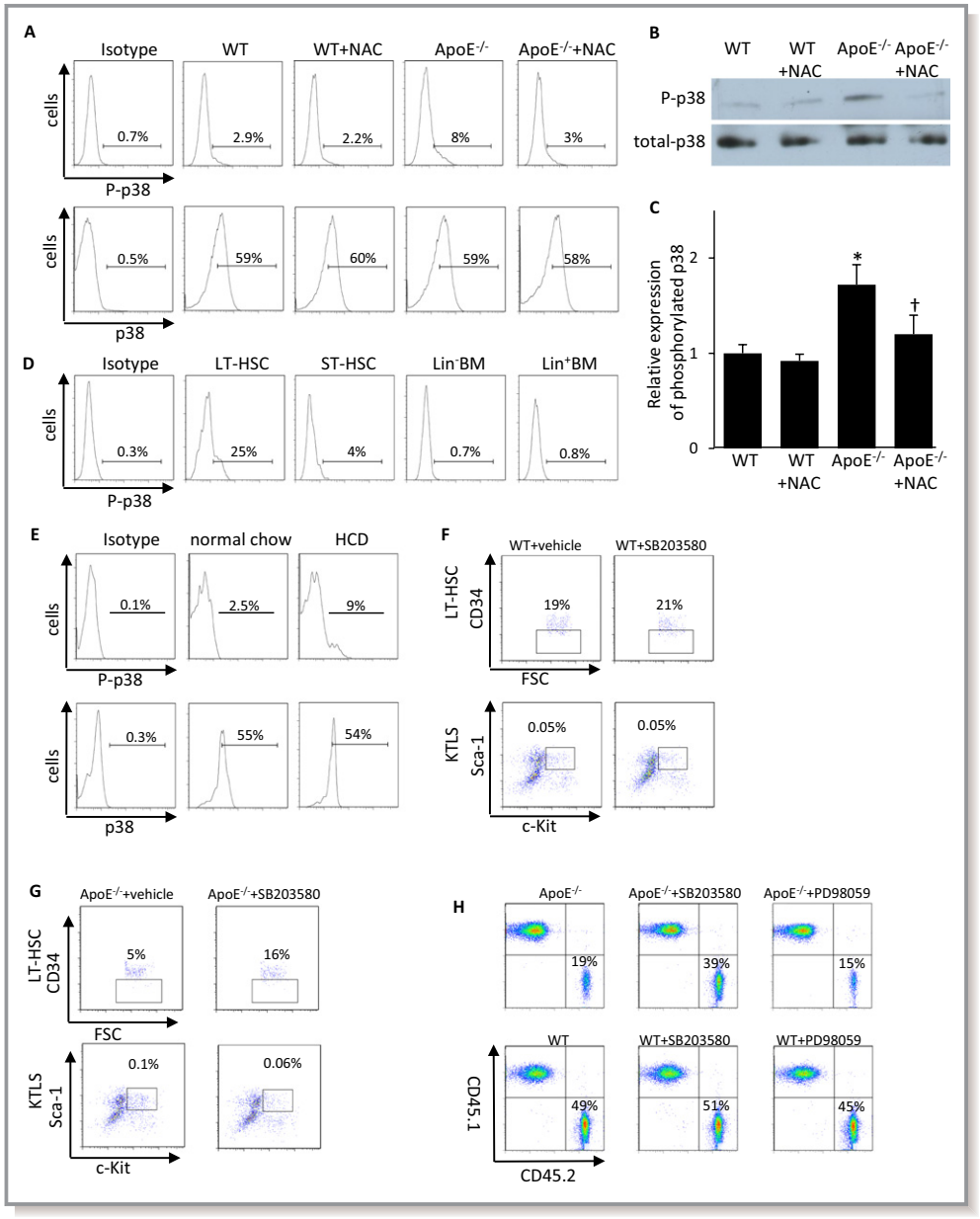

Figure 9. Hypercholesterolemia increases the activity of p38 MAPK in HSCs. A, Phosphorylated p38 expression was measured by Flowcytometry in KTLS cells from WT mice (2.7±0.9%), NAC treated WT mice (2.1±.7%), ApoE$^{-/-}$ mice (8.4±0.6% *) and NAC treated ApoE$^{-/-}$ mice (2.7±0.9% †). Total p38 did not show difference in KTLS cells from WT mice (59.7±2.4%), NAC treated WT mice (60.2±4.5%), ApoE$^{-/-}$ mice (57±2.6%) and NAC treated ApoE$^{-/-}$ mice (58.3±1.8%). The numbers represent M±SD (n=6, *P<0.05 vs WT; †P<0.05 vs ApoE$^{-/-}$). B and C, Phosphorylated and total p38 expression was measured by Western blot (B) in KTLS cells from WT mice, NAC treated WT, ApoE$^{-/-}$, and NAC treated ApoE$^{-/-}$ mice. The results was quantified (C) (n=3, *P<0.05, vs WT; †P<0.05, vs ApoE$^{-/-}$ mice). D, Phosphorylated p38 expression was measured by Flowcytometry in phenotypically defined LT (24.2±.8% *†) and ST-HSC (3.9±.4% *) as well as Lin^{-} (0.7±0.2%) and Lin^{+} marrow cells (0.8±0.3%) from ApoE$^{-/-}$ mice (n=6, *P<0.05 vs Lin^{-}, †P<0.05 vs Lin^{+}). E, Phosphorylated p38 expression was measured by Flowcytometry in KTLS cells from normal chow mice (2.5±0.3%) and HCD mice (9.8±1.9% *). Total p38 did not show difference between normal chow mice (55.2±4.5%) and HCD mice (53.6±3.9%). The numbers represent M±SD. (n=6, *P<0.05 vs WT). F, The frequency of phenotypically defined LT-HSC in total KTLS population was measured by Flowcytometry in WT (19±0.8%) and SB203580 treated WT mice (22±2%). The frequency of KTLS cells in total bone marrow was measured by Flowcytometry in WT mice (0.053±0.01%) and SB203580 treated WT mice (0.051±0.006%). The numbers represent M±SD (n=6). G, The frequency of phenotypically defined LT-HSC in total KTLS population was measured by Flowcytometry in ApoE$^{-/-}$ (5.39±1.8%) and SB203580 treated ApoE$^{-/-}$ mice (15.6±3.3% *). The frequency of KTLS cells in total bone marrow was measured by Flowcytometry in ApoE$^{-/-}$ (0.102±0.01%) and SB203580 treated ApoE$^{-/-}$ mice (0.067±0.008% *). (n=6, *P<0.05 vs ApoE$^{-/-}$). H, Competitive HSC transplantation assay of KTLS cells from WT (49.6±2.4% *), SB203580 treated WT (50.1±5.6% *), PD98059 treated WT(45.1±4.9% *), ApoE$^{-/-}$ (19.3±2.4%), SB203580 treated ApoE$^{-/-}$ (38.9±103% *), PD98059 treated ApoE$^{-/-}$ mice (18.2±7.7%). The percent of CD45.2^{+} cells in total KTLS were represented as M±SD (n=8, *P<0.05, vs ApoE$^{-/-}$). BM indicates bone marrow; HCD, high cholesterol diet; HSCs, hematopoietic stem cells; LT, long-term; NAC, *N*-acetylcysteine; ST, short term; WT, wild type.

A

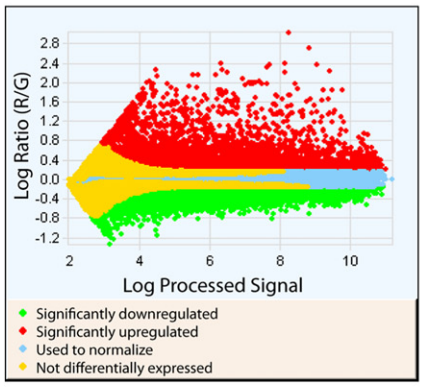

B

Name	*p-value*
P53/P21 Signaling	5.55E-05
Cell Cycle: G/M DNA Damage Checkpoint Regulation	1.12E-03
IL-8 Signaling	2.65E-03
One Carbon Pool by Folate	3.11E-03

C

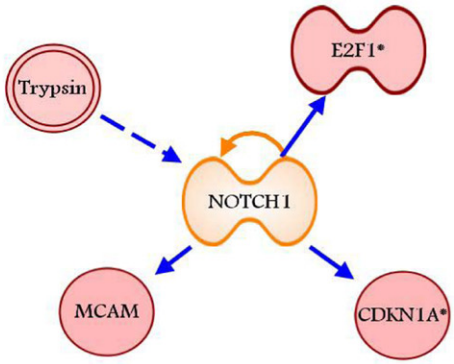

Figure 10. The effect of hypercholesterolemia on HSC gene expression. A, Representative plot of log ratio vs log processed signal in ApoE$^{-/-}$ vs WT HSC for all the 44 000 probes present on the microarray (n=3). B, The top 4 canonical pathways determined by Ingenuity Pathways analysis based on differentially expressed genes in HSC from ApoE$^{-/-}$ vs WT mice. C, Ingenuity Pathway analysis showed increases in the expression of several important components in Notch signaling, including E2F1, MCAM, CDKN1A, and trypsin. CDKN1A indicates cyclin-dependent kinase inhibitor 1; HSC, hematopoietic stem cell; MCAM, melanoma cell adhesion molecule; WT, wild type.

limited number enter the cell cycle, which is driven by both extrinsic and intrinsic cues. Recent studies showed that increased oxidant stress exerts a critical role in the regulation of HSC quiescence and function.[13,16] In the present study, we found that HSCs isolated from two different mouse models of hypercholesterolemia possessed abnormal accumulation of ROS, while ROS levels in total bone marrow cells were similar in hypercholesterolemic mice and WT mice, indicating that hypercholesterolemia induces oxidant stress specifically in HSCs. PCR array analysis confirmed an aberrant expression of a subset of ROS genes in HSCs isolated from hypercholesterolemic mice. The long-term treatment with antioxidants, NAC and GSH, effectively decreased oxidant stress, and restored the quiescence as well as the reconstitution capacity of HSCs from hypercholesterolemic mice. This effect was present in a well-established mouse model of hypercholesterolemia (ApoE$^{-/-}$), as well in C57Bl/6 mice in whom hypercholesterolemia was diet-induced; thus, it is clear that hypercholesterolemia causes oxidant stress and impairs the quiescence and function of HSCs. The importance of the present findings is that it extends the known deleterious effects of hypercholesterolemia to HSCs, a common clinical entity and one that has clear impact on morbidity and mortality.[1–3]

A previous study showed that antioxidant GSH reversed IL-3 induced abnormal myelopoiesis of total bone marrow cells isolated from hypercholesterolemic ABCA1$^{-/-}$ABCG1$^{-/-}$ mice, but it failed to reverse the abnormal myelopoiesis with antioxidant NAC.[10] However, in that study, total bone marrow cells rather than HSCs were studied. In addition, myelopoiesis of total bone marrow mononuclear cells was measured 72 hours after their harvest in an in vitro assay. In this study, oxidant stress was measured in HSCs. These differences in techniques and experimental design could account for the different observations between this study and the other published studies.

Based on the exaggerated monocytosis, spleen size, and serum cholesterol level found in HFD fed ApoE$^{-/-}$ mice, we hypothesized that HFD mice caused marked systemic inflammation in ApoE$^{-/-}$ mice that resulted in extramedullary hematopoiesis and monocytosis. A very recent study supports this explanation of the findings.[17] The study indicated that HFD caused a similar, very significant monocytosis and accelerated atherosclerosis in ApoE$^{-/-}$ mice in response to inflammation. Furthermore, this phenotype was largely attributed to extramedullary hematopoiesis in spleen, rather than the changes of HSCs in the bone marrow. Obviously, the total serum cholesterol levels of almost 1,000 mg/dl in HCD fed ApoE$^{-/-}$ mice are extraordinarily high and have much less clinical relevance than do the levels in our study, ≈240 mg/dL. These findings suggest caution while investigating the effects of hypercholesterolemia on hematopoiesis or HSCs in ApoE$^{-/-}$ mice fed a HFD, due to these extraordinarily high serum cholesterol levels and attendant systemic inflammation.

These previous studies also showed that hypercholesterolemic ABCA1- and ABCG1-deficient mice as well as ApoE$^{-/-}$

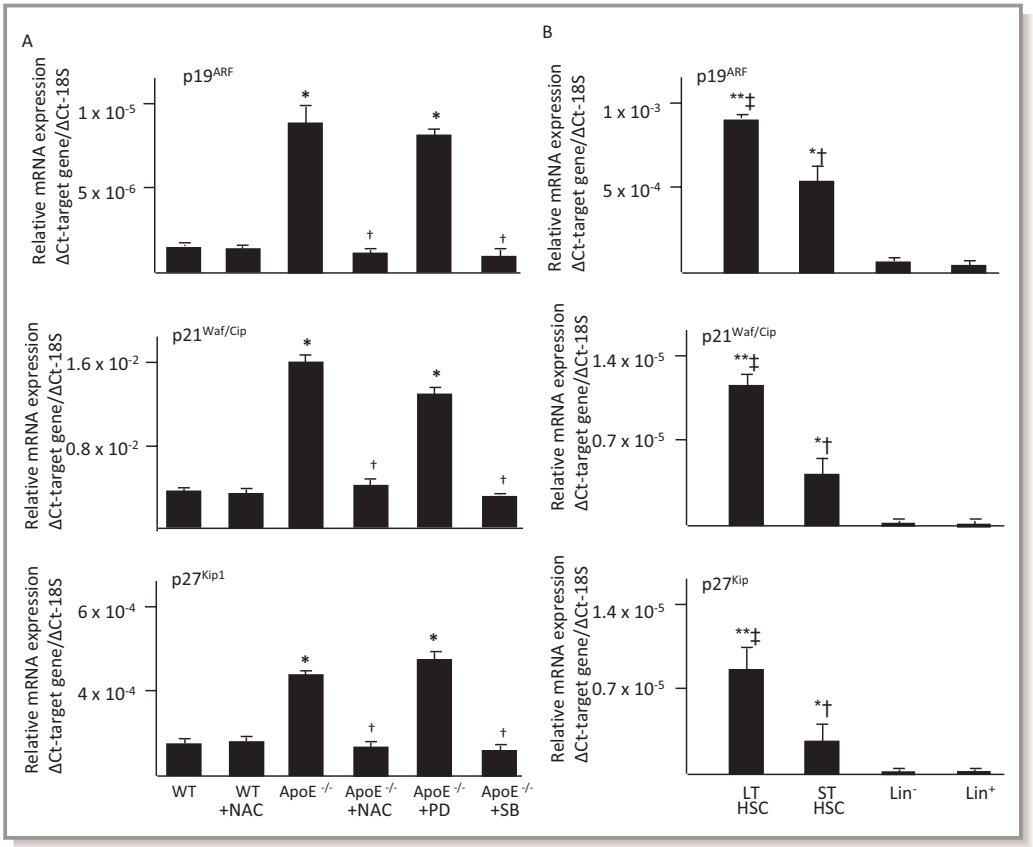

Figure 11. Hypercholesterolemia causes a paradoxical increase in expression of cell cycle inhibitors via oxidant-dependent increase in p38 activity. A, *p19*^{Arf}, *p21*^{Waf1}, and *p27*^{Kip1} expression in HSCs from WT mice, NAC treated WT mice, ApoE$^{-/-}$ mice, NAC treated ApoE$^{-/-}$ mice, MEK1 inhibitor PD98059 treated ApoE$^{-/-}$ mice, and p38 inhibitor SB203580 treated ApoE$^{-/-}$ mice (n=6, **P*<0.05 vs WT, †*P*<0.05 vs ApoE$^{-/-}$). B, *p19*^{Arf}, *p21*^{Waf1}, and *p27*^{Kip1} expression in phenotypically defined LT- and ST-HSC as well as Lin^{-} and Lin^{+} bone marrow cells from ApoE$^{-/-}$ mice (n=6, ***P*<0.01 vs Lin^{-}, ‡*P*<0.01 vs Lin^{+}, **P*<0.05 vs Lin^{-}, †*P*<0.05 vs Lin^{-}). HSCs indicates hematopoietic stem cells; LT, long-term; MEK, mitogen activated protein kinase kinase; NAC, *N*-acetylcysteine; ST, short term; WT, wild type.

mice fed a western diet displayed a dramatic expansion of HSCs in the bone marrow.[10,11] These studies suggest that the abnormal expansion of the HSC compartment was related to an increased membrane cholesterol content that induces increased cell-surface IL-3 or GM-CSF receptors and thereby increases the HSC proliferative response to IL-3 and GM-CSF. However, these studies did not address the question if hypercholesterolemia accelerates ageing in hematopoietic progenitor/stem cells. In agreement with the clinical investigations,[4,10] our results showed hypercholesterolemia-induced oxidant stress that caused loss of quiescence in the HSC compartment, evidenced by increased proportion of phenotypically defined ST-HSCs within the bone marrow, reduced proportion of phenotypically defined LT-HSC and side population as well as telomere shortening and reduced reconstitution capacity of HSC population. Our findings indicate that hypercholesterolemia accelerates ageing in HSCs in oxidant stress dependent manner, which cause the loss of quiescence of LT-HSC compartment, force more LT-HSCs into cell cycle, and result in telomere erosion and expansion of ST-HSC compartment with expense of impaired reconstitution capacity of HSCs in hypercholesterolemic mice.

We have found that oxidant stress in bone marrow cells of hypercholesterolemic mice occurs in a cell type-specific manner. Interestingly, although HSCs express LOX-1, this expression was significantly lower in HSCs than in other bone marrow cells. It is well established that most HSCs are quiescent in the bone marrow. Therefore, the lower expression of LOX-1 in the HSC compartment may protect HSCs from accumulation of oxLDL and secondary oxidant stress. A previous study reported similar cell type specific changes that were consistent with the protection of HSCs from oxidant stress. In this study, ABCA1 and ABCG1 were expressed at much higher levels in HSCs than other bone marrow cells.[10] The cell type-specific differences in the sensitivity of bone marrow cells to oxidant stress may also be related to differences in the HSC microenvironment. For example, HSCs reside in a relatively hypoxic area of the bone marrow and therefore may not have

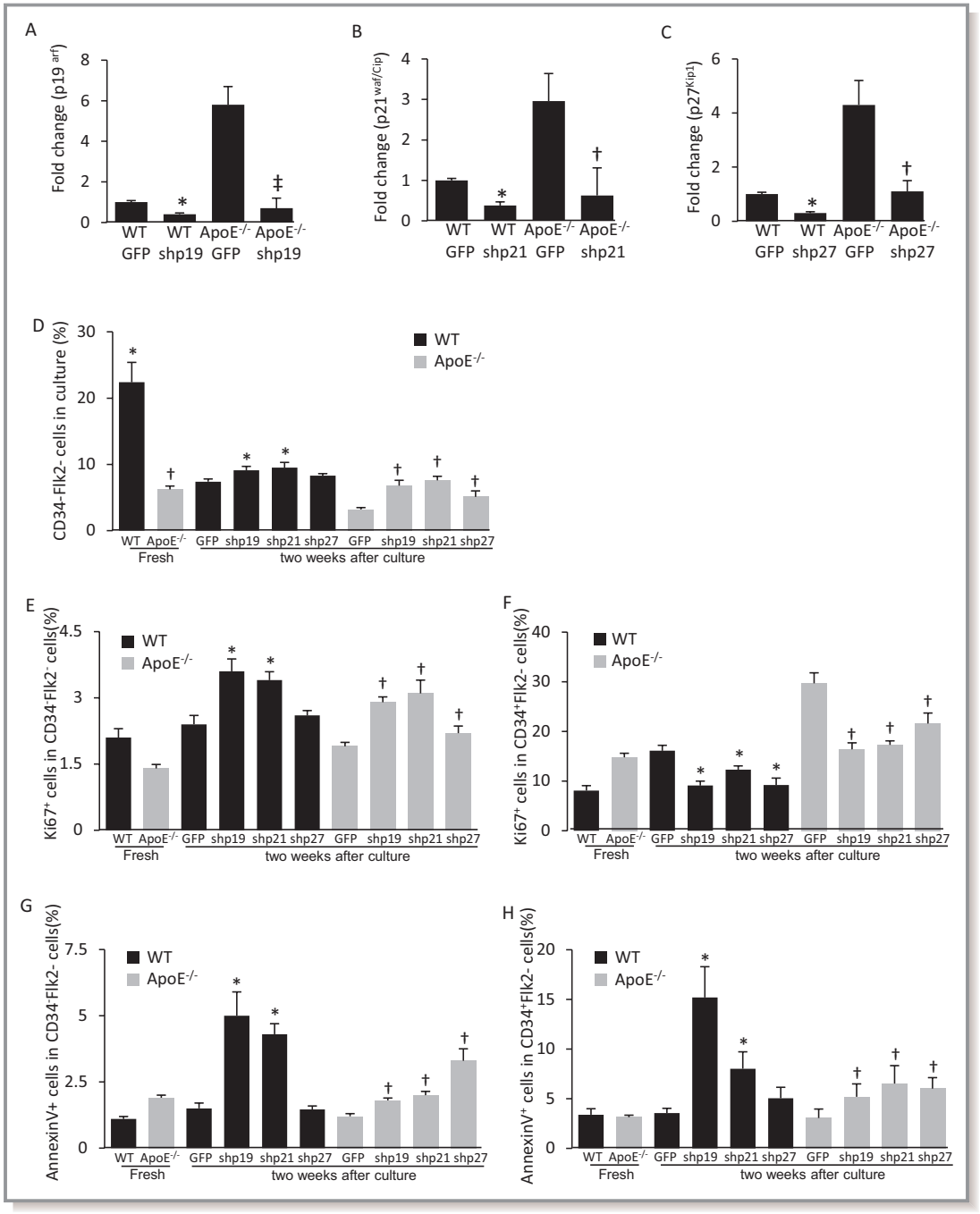

Figure 12. Inhibition of $p19^{Arf}$, $p21^{Waf1}$, and $p27^{Kip1}$ increases phenotypically defined long term population in KTLS culture in vitro. A, Expression of $p19^{Arf}$ in KTLS cells after Lenti-shp19 transfection (n=6, *P<0.05 vs WT, ‡P<0.01 vs ApoE$^{-/-}$). B, Expression of $p21^{Waf1}$ in KTLS cells after Lenti-shp21 transfection (n=6, *P<0.05 vs WT, †P<0.05 vs ApoE$^{-/-}$). C, Expression of $p27^{Kip1}$ in KTLS cells after Lenti-shp27 transfection (n=6, *P<0.05 vs WT, †P<0.05 vs ApoE$^{-/-}$). D, CD34$^-$Flk$_2^-$ cells in fresh KTLS or in total KTLS culture 2 weeks after Lentiviral transfection (M±SD, n=6, *P<0.05 vs WT GFP, †P<0.05 vs ApoE$^{-/-}$ GFP). E, Ki67$^+$ cells in fresh CD34$^-$Flk$_2^-$KTLS or in cultured CD34$^-$Flk$_2^-$KTLS 2 weeks after Lentiviral transfection (M±SD, n=6, *P<0.05 vs WT GFP, †P<0.05 vs ApoE$^{-/-}$ GFP). F, Ki67$^+$ cells in fresh CD34$^+$Flk$_2^-$KTLS or in cultured CD34$^+$Flk$_2^-$KTLS 2 weeks after Lentiviral transfection (M±SD, n=6, *P<0.05 vs WT GFP, †P<0.05 vs ApoE$^{-/-}$ GFP). G, Annexin V$^+$ cells in fresh CD34$^-$Flk$_2^-$KTLS or in cultured CD34$^-$Flk$_2^-$KTLS 2 weeks after Lentiviral transfection (M±SD, n=6, *P<0.05 vs WT GFP, †P<0.05 vs ApoE$^{-/-}$ GFP). H, Annexin V$^+$ cells in fresh CD34$^+$Flk$_2^-$KTLS or in cultured CD34$^+$Flk$_2^-$KTLS 2 weeks after Lentiviral transfection (M±SD, n=6, *P<0.05 vs WT GFP, †P<0.05 vs ApoE$^{-/-}$ GFP). WT indicates wild type.

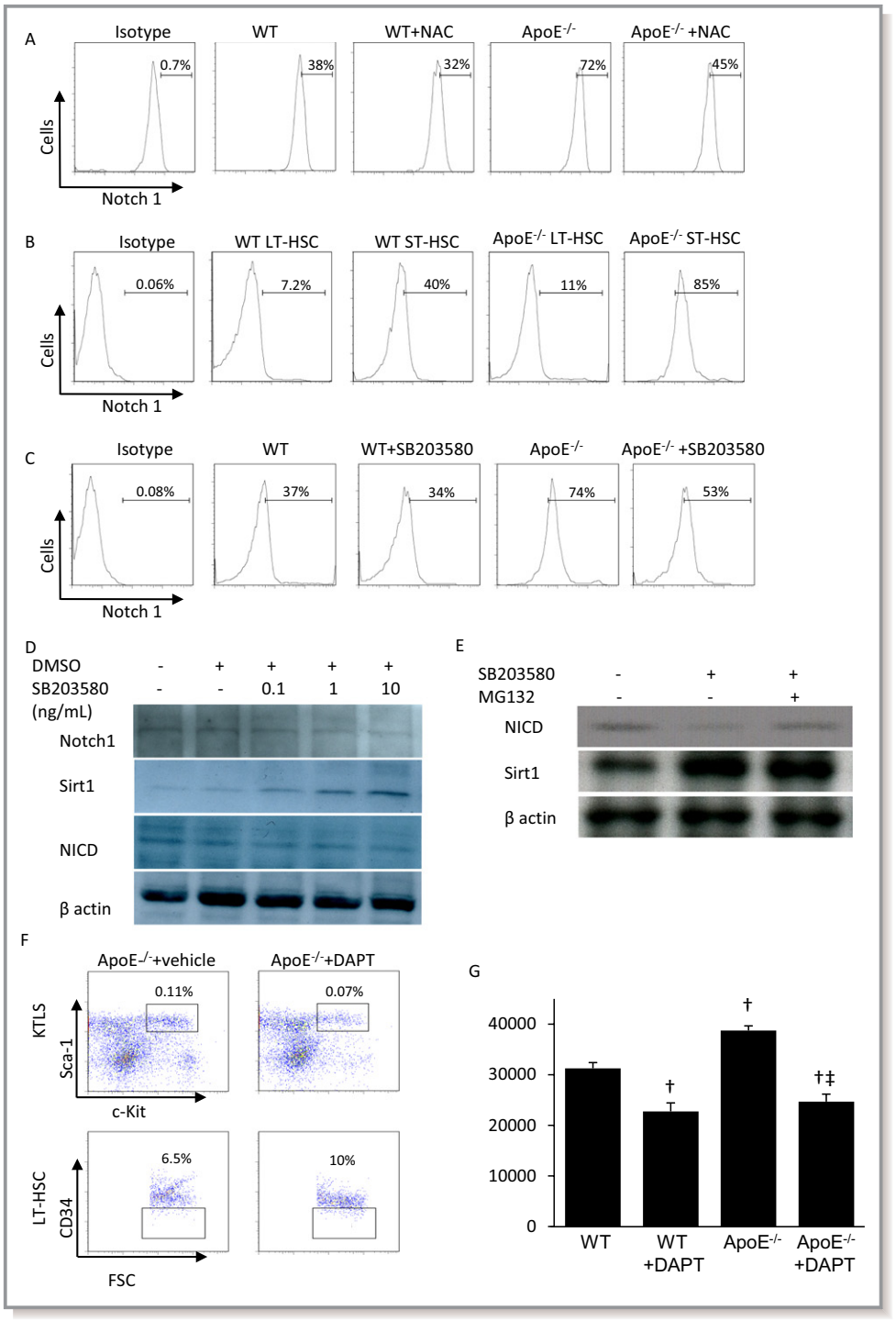

Figure 13. Hypercholesterolemia-induced oxidant stress increases Notch1 activity in a p38-dependent manner that contributes to HSC ageing. A, Notch1 expression in KTLS cells from WT mice (37.7±5.1%), NAC-treated mice (31.5±2.7%), ApoE$^{-/-}$ (70.8±.6% *) and NAC-treated ApoE$^{-/-}$ mice (46.5±11.3% †). The numbers represent M±SD. (n=8, *P<0.05 vs WT, †P<0.05 vs ApoE$^{-/-}$). B, Notch1 expression in phenotypically defined LT-HSC (7.3±1.8%) and ST-HSC (39.4±4.5%) from WT mice as well as LT-HSC (10.2±2.7%) and ST-HSC (82.7±9.5% *) from ApoE$^{-/-}$ mice (M±SD, n=8, *P<0.05 vs WT ST-HSC). C, Notch1 expression in KTLS cells from WT (36.3±2.8%), SB203580 treated WT (33.4±3.7%), ApoE$^{-/-}$ mice (72.9±6.3% *), and SB203580 treated ApoE$^{-/-}$ mice (51.1±11% †) (n=8, *P<0.05 vs WT, †P<0.05 vs ApoE$^{-/-}$). D, Notch1, Sirt1, and Notch1 intracellular domain (NICD) expression in WT KTLS cells after in vitro SB203580 treatment (n=3). E, Notch1 intracellular domain and Sirt1 expression in WT KTLS cells after in vitro treatment with p38 inhibitor SB203580 and/or Sirt1 inhibitor MG132 (n=3). F, Frequency of KTLS in bone marrow of ApoE$^{-/-}$ mice (0.11±0.01%) and DAPT treated ApoE$^{-/-}$ mice (0.08±0.01†). Phenotypically defined LT-HSC in KTLS population of ApoE$^{-/-}$ mice (6.5±1.4%) and DAPT treated ApoE$^{-/-}$ mice (10.8±1.9% †) (n=6, †P<0.05). G, The inhibition of KTLS expansion in vitro by DAPT. KTLS cells from WT and ApoE$^{-/-}$ mice were treated with DAPT in vitro and HSC expansion was quantified (n=6, †P<0.05 vs WT, ‡P<0.05 vs ApoE$^{-/-}$). DAPT indicates N-[N-(3,5-Difluorophenacetyl)-L-alanyl]-S-phenylglycinet-butyl ester; DMSO, dimethyl sulfoxide; HSC, hematopoietic stem cell; LT-HSC, long-term HSC; NAC, *N*-acetylcysteine; ST-HSC, short term HSC; WT, wild type.

robust antioxidant defense systems. In support of this hypothesis, we found HSCs of ApoE$^{-/-}$ mice displayed an unexpected pattern of downregulation of many antioxidant genes.

To elucidate the mechanism underlying the effects of hypercholesterolemia on HSC quiescence and reconstitution capacity, we focused on the Cip/Kip and Ink4 cell cycle inhibitor families, which maintain the quiescence of HSCs, thereby governing their available pool size.[18–20] In the present study, *p19^{ARF}*, *p21^{Waf1}*, and *p27^{Kip1}* were paradoxically upregulated in HSCs from hypercholesterolemic mice. Among the Cip/Kip family, *p21^{Waf1}* has been suggested to play a key role in the maintenance of HSC quiescence and pool size.[18,21] *P21^{Waf1}* also displays a differentiation stage-specific function in hematopoietic stem cells. *P21^{Waf1}* inhibits the proliferation of quiescent stem cells, while it has a paradoxical proliferative effect on more mature stem and progenitor cells.[18,21] Similar paradoxical changes to those documented in our study were also observed in ATM-deficient mice in which this genetic deletion induced HSC oxidant stress.[12,13,22] Increased *p16^{Ink1}*, one important member of INK family, was verified to be responsible for a decreased cKit^{hi}Sca1^{+}Lin^{-} population[13] while the cKit^{lo}Sca1^{+}Lin^{-} compartment was increased in ATM-deficient mice.[10,20] It has been shown that *p19^{ARF}* decreases the size of phenotypically defined LT-HSC compartment without inducing apoptosis.[13] This study also supports our findings in ApoE$^{-/-}$ mice that activation of *p19^{ARF}* decreases the size of phenotypically defined LT-HSC compartment. When treated with NAC, the increased expression of *p19^{ARF}*, *p21^{Waf1}*, and *p27^{Kip1}* in HSCs from hypercholesterolemic mice was reduced. Inhibition of *p19^{Arf}*, *p21^{Waf1}*, and *p27^{Kip1}* significantly increased CD34^{-}Flk$_2^{-}$ populations in KTLS culture. The results indicated that hypercholesterolemia-induced oxidant stress caused aberrant expression of the Ink4 and Cip/Kip CKI families, subsequently decreasing HSC quiescence and LT-HSC population, impairing reconstitution capacity, and accelerating the ageing of HSCs.

P38 MAPK mediates the stress responses in a variety of cells under conditions of oxidant stress.[23,24] Our results showed that p38 phosphorylation was significantly higher in the HSCs from hypercholesterolemic mice. The inhibition of p38 restored the quiescence and reconstitution capacity of HSCs in hypercholesterolemic mice. It has also been shown that the Cip/Kip and Ink4 families are regulated by MAPKs, including p38 and Erk.[25–27] In concordance with these results, the inhibition of p38 also rescued the aberrant expression of the Ink4 and Cip/Kip families in hypercholesterolemic mice. These results indicated that hypercholesterolemia-induced oxidant stress increased phosphorylation of p38 in HSCs from hypercholesterolemic mice was central to the loss of quiescence and repopulation capacity.

We also found a significant increase in the expression of Notch1 in HSCs from hypercholesterolemic mice. Notch1 expression was decreased in HSCs after inhibition of p38 MAPK in vivo and in vitro. In addition, p38 inhibitor SB203580 upregulated the expression of Sirt1, which has been shown to negatively modulate Notch activity in HSCs.[28] These results reinforce that the p38 pathway also augments the activity of Notch1 under conditions of hypercholesterolemia-induced oxidant stress. It has been shown that exposure of HSCs to Notch ligand induces their self-renewal and expansion.[29] We found that treatment with DAPT significantly decreased the HSC compartment in vivo and the proliferation of HSCs from hypercholesterolemic mice in vitro. These results indicate that the p38-dependent increase in Notch1 activity contributes to expansion of the HSC compartment in hypercholesterolemic mice.

Taken together, we provide evidence that hypercholesterolemia can cause oxidant stress that accelerates the ageing and impairs the reconstitution capacity of HSCs. The novel mechanism identified in the present study should lead to additional studies to determine if hypercholesterolemia-induced oxidant stress also impairs HSC differentiation and thereby affect immunity and inflammation. Such findings could lead to new insights into the mechanisms by which hypercholesterolemia increases all-cause mortality.

Acknowledgments

We thank J. Witztum and R. Raffai for their gifts of oxLDL antibody.

Author Contributions

Drs Tie, K. Messina, Yan, and J. Messina designed and performed the experiments. Dr L. Messina conceived and supervised the whole project. All authors discussed the results and commented on the manuscript.

Sources of Funding

This work was supported by a grant from US National Institutes of Health RO-1 HL 75353 (to Dr L. Messina).

Disclosures

None.

References

1. Barter P, Gotto AM, LaRosa JC, Maroni J, Szarek M, Grundy SM, Kastelein JJ, Bittner V, Fruchart JC. HDL cholesterol, very low levels of LDL cholesterol, and cardiovascular events. *N Engl J Med*. 2007;357:1301–1310.
2. Goldbourt U, Holtzman E, Neufeld HN. Total and high density lipoprotein cholesterol in the serum and risk of mortality: evidence of a threshold effect. *Br Med J (Clin Res Ed)*. 1985;290:1239–1243.
3. Chyou P, Eaker HED. Serum cholesterol concentrations and all-cause mortality in older people. *Age Ageing*. 2000;29:69–74.

4. Poch E, Carbonell P, Franco S, Diez-Juan A, Blasco MA, Andres V. Short telomeres protect from diet-induced atherosclerosis in apolipoprotein E-null mice. *FASEB J*. 2004;18:418–420.
5. Spyridopoulos I, Erben Y, Brummendorf TH, Haendeler J, Dietz K, Seeger F, Kissel CK, Martin H, Hoffmann J, Assmus B, Zeiher AM, Dimmeler S. Telomere gap between granulocytes and lymphocytes is a determinant for hematopoetic progenitor cell impairment in patients with previous myocardial infarction. *Arterioscler Thromb Vasc Biol*. 2008;28:968–974.
6. Harley CB, Futcher AB, Greider CW. Telomeres shorten during ageing of human fibroblasts. *Nature*. 1990;345:458–460.
7. Saliques S, Zeller M, Lorin J, Lorgis L, Teyssier JR, Cottin Y, Rochette L, Vergely C. Telomere length and cardiovascular disease. *Arch Cardiovasc Dis*. 2010;103:454–459.
8. Coller BS. Leukocytosis and ischemic vascular disease morbidity and mortality: is it time to intervene? *Arterioscler Thromb Vasc Biol*. 2005;25:658–670.
9. Gordon DJ, Rifkind BM. High-density lipoprotein—the clinical implications of recent studies. *N Engl J Med*. 1989;321:1311–1316.
10. Yvan-Charvet L, Pagler T, Gautier EL, Avagyan S, Siry RL, Han S, Welch CL, Wang N, Randolph GJ, Snoeck HW, Tall AR. ATP-binding cassette transporters and HDL suppress hematopoietic stem cell proliferation. *Science*. 2010;328:1689–1693.
11. Murphy AJ, Akhtari M, Tolani S, Pagler T, Bijl N, Kuo CL, Wang M, Sanson M, Abramowicz S, Welch C, Bochem AE, Kuivenhoven JA, Yvan-Charvet L, Tall AR. ApoE regulates hematopoietic stem cell proliferation, monocytosis, and monocyte accumulation in atherosclerotic lesions in mice. *J Clin Invest*. 2011;121:4138–4149.
12. Ito K, Hirao A, Arai F, Matsuoka S, Takubo K, Hamaguchi I, Nomiyama K, Hosokawa K, Sakurada K, Nakagata N, Ikeda Y, Mak TW, Suda T. Regulation of oxidative stress by ATM is required for self-renewal of haematopoietic stem cells. *Nature*. 2004;431:997–1002.
13. Ito K, Hirao A, Arai F, Takubo K, Matsuoka S, Miyamoto K, Ohmura M, Naka K, Hosokawa K, Ikeda Y, Suda T. Reactive oxygen species act through p38 MAPK to limit the lifespan of hematopoietic stem cells. *Nat Med*. 2006;12:446–451.
14. Owens AP III, Passam FH, Antoniak S, Marshall SM, McDaniel AL, Rudel L, Williams JC, Hubbard BK, Dutton JA, Wang J, Tobias PS, Curtiss LK, Daugherty A, Kirchhofer D, Luyendyk JP, Moriarty PM, Nagarajan S, Furie BC, Furie B, Johns DG, Temel RE, Mackman N. Monocyte tissue factor-dependent activation of coagulation in hypercholesterolemic mice and monkeys is inhibited by simvastatin. *J Clin Invest*. 2012;122:558–568.
15. Osawa M, Hanada K, Hamada H, Nakauchi H. Long-term lymphohematopoietic reconstitution by a single CD34-low/negative hematopoietic stem cell. *Science*. 1996;273:242–245.
16. Balaban RS, Nemoto S, Finkel T. Mitochondria, oxidants, and ageing. *Cell*. 2005;120:483–495.
17. Dutta P, Courties G, Wei Y, Leuschner F, Gorbatov R, Robbins CS, Iwamoto Y, Thompson B, Carlson AL, Heidt T, Majmudar MD, Lasitschka F, Etzrodt M, Waterman P, Waring MT, Chicoine AT, van der Laan AM, Niessen HW, Piek JJ, Rubin BB, Butany J, Stone JR, Katus HA, Murphy SA, Morrow DA, Sabatine MS, Vinegoni C, Moskowitz MA, Pittet MJ, Libby P, Lin CP, Swirski FK, Weissleder R, Nahrendorf M. Myocardial infarction accelerates atherosclerosis. *Nature*. 2012;487:325–329.
18. Cheng T, Rodrigues N, Shen H, Yang Y, Dombkowski D, Sykes M, Scadden DT. Hematopoietic stem cell quiescence maintained by p21cip1/waf1. *Science*. 2000;287:1804–1808.
19. Cheng T, Rodrigues N, Dombkowski D, Stier S, Scadden DT. Stem cell repopulation efficiency but not pool size is governed by p27(kip1). *Nat Med*. 2000;6:1235–1240.
20. Walkley CR, Fero ML, Chien WM, Purton LE, McArthur GA. Negative cell-cycle regulators cooperatively control self-renewal and differentiation of haematopoietic stem cells. *Nat Cell Biol*. 2005;7:172–178.
21. Mantel C, Luo Z, Canfield J, Braun S, Deng C, Broxmeyer HE. Involvement of p21cip-1 and p27kip-1 in the molecular mechanisms of steel factor-induced proliferative synergy in vitro and of p21cip-1 in the maintenance of stem/progenitor cells in vivo. *Blood*. 1996;88:3710–3719.
22. Hishiya A, Ito M, Aburatani H, Motoyama N, Ikeda K, Watanabe K. Ataxia telangiectasia mutated (Atm) knockout mice as a model of osteopenia due to impaired bone formation. *Bone*. 2005;37:497–503.
23. Deng Q, Liao R, Wu BL, Sun P. High intensity ras signaling induces premature senescence by activating p38 pathway in primary human fibroblasts. *J Biol Chem*. 2004;279:1050–1059.
24. Wang WJ, Chen X, Liao R, Deng Q, Zhou JJ, Huang S, Sun P. Sequential activation of the MEK-extracellular signal-regulated kinase and MKK3/6-p38 mitogen-activated protein kinase pathways mediates oncogenic ras-induced premature senescence. *Mol Cell Biol*. 2002;22:3389–3403.
25. Aghdasi B, Ye K, Resnick A, Huang A, Ha HC, Guo X, Dawson TM, Dawson VL, Snyder SH. FKBP12, the 12-kDa FK506-binding protein, is a physiologic regulator of the cell cycle. *Proc Natl Acad Sci USA*. 2001;98:2425–2430.
26. Bulavin DV, Phillips C, Nannenga B, Timofeev O, Donehower LA, Anderson CW, Appella E, Fornace AJ Jr. Inactivation of the Wip1 phosphatase inhibits mammary tumorigenesis through p38 MAPK-mediated activation of the p16 (Ink4a)-p19(Arf) pathway. *Nat Genet*. 2004;36:343–350.
27. Choi BH, Kim CG, Bae YS, Lim Y, Lee YH, Shin SY. p21 Waf1/Cip1 expression by curcumin in U-87MG human glioma cells: role of early growth response-1 expression. *Cancer Res*. 2008;68:1369–1377.
28. Guarani V, Deflorian G, Franco CA, Kruger M, Phng LK, Bentley K, Toussaint L, Dequiedt F, Mostoslavsky R, Schmidt MH, Zimmermann B, Brandes RP, Mione M, Westphal CH, Braun T, Zeiher AM, Gerhardt H, Dimmeler S, Potente M. Acetylation-dependent regulation of endothelial Notch signalling by the SIRT1 deacetylase. *Nature*. 2011;473:234–238.
29. Varnum-Finney BL, Purton E, Yu M, Brashem-Stein C, Flowers D, Staats S, Moore KA, Le Roux I, Mann R, Gray G, Artavanis-Tsakonas S, Bernstein ID. The Notch ligand, Jagged-1, influences the development of primitive hematopoietic precursor cells. *Blood*. 1998;91:4084–4091.